

Dynamical back-reaction of relic gravitons

Massimo Giovannini ¹

Centro "Enrico Fermi", Compendio del Viminale, Via Panisperna 89/A, 00184 Rome, Italy

Department of Physics, Theory Division, CERN, 1211 Geneva 23, Switzerland

Abstract

The dynamical effects of the tensor modes of the geometry are investigated in the context of curvature bounces. Since the bouncing behaviour implies sharp deviations from a radiation-dominated evolution, significant back-reaction effects of relic gravitons may be expected at short wavelengths. After developing a general iterative framework for the calculation of dynamical back-reaction effects, explicit analytical and numerical examples are investigated for different parametrizations of the energy-momentum pseudo-tensor(s) of the produced gravitons. The reported results suggest that dynamical back-reaction effects are a necessary ingredient for a consistent description of bouncing models at late times.

¹e-mail address: massimo.giovannini@cern.ch

1 Introduction

Relic gravitons are copiously produced in the early Universe due to the pumping action of the background geometry [1, 2]. If a quasi-de Sitter phase of expansion is followed by a radiation-dominated phase, the logarithmic energy spectrum (in units of the critical energy density), customarily denoted by $\Omega_{\text{gw}}(\nu)$, is quasi-flat [3] (see also [4, 5, 6]) for present (physical) frequencies ν ranging between 10^{-16} Hz and, approximately, 100 MHz. The transition from the radiation-dominated to the matter epoch produces an infrared branch where $\Omega_{\text{gw}} \sim \nu^{-2}$ between 10^{-18} Hz and 10^{-16} Hz [7, 8, 9].

In pre-big bang models [10, 11], the spectrum of relic gravitons is far from scale-invariant. The spectral slope of $\Omega_{\text{gw}}(\nu)$ (for frequencies larger than 10^{-16} Hz) is violet, i.e. $\Omega_{\text{gw}} \sim \nu^\gamma$ with $\gamma > 1$ [5, 12] (see also [13] and, in a complementary perspective, [14]). Minimal pre-big bang models are characterized by a slope $\gamma = 3$ that become progressively less steep as the frequency increases in the kHz and MHz region.

Depending on the features of the cosmological model, the energy density of relic gravitons may affect the dynamics and change the time evolution of the scale factor as well as of the other homogeneous quantities. If the equation of state of the sources of the background geometry is stiffer than radiation (i.e. $p = w\rho$ with $w > 1/3$) the relativistic gravitons of short wavelengths can change the dynamical evolution, as it was noticed in the context of the stiff model of Zeldovich [2].

When a stiff phase follows an inflationary stage of expansion [15] (see also [16, 17]²) the back-reaction effects of the produced gravitons set a limit on the possible duration of the stiff (post-inflationary) phase. This aspect is relevant in different situations and, for instance, in the context of quintessential inflationary models [20] where $\Omega_{\text{gw}} \propto \nu$ for frequencies larger than the mHz [22, 23, 24] (see also [25, 26, 27, 28] for possible detection strategies). Blue spectral slopes have been also derived in the context of quintessential models on the brane [29, 30] (see also [31]). Constraints arising from the production of relic gravitons in quintessential models have been discussed in [32].

Defining as τ the conformal time coordinate and k as the comoving wave-number, two physically different regimes appear naturally in the problem. If $k\tau \ll 1$ (short wavelength limit) the Fourier modes of the tensor fluctuations of the geometry are said to be super-adiabatically amplified. In the opposite regime, i.e. $k\tau \gg 1$ (long wavelength limit) the tensor modes are oscillating. In the

²It is relevant to remark that the authors of Refs. [16] and [17] choose to compute the energy and pressure density of the produced particles by means of a perturbative expansion whose small parameter is the deviation from conformal coupling ($|\xi - 1/6|$ in the notations of [17]). This approach (also discussed in [18, 19]) may be applied, with some caveats, in the minimally coupled case (corresponding to $\xi \rightarrow 0$) where, it could be argued that the expansion parameter does not exceed 1. In the present investigation this expansion will not be used since the coupling of relic gravitons to the background geometry is not close to conformal. Furthermore the expansion in $|\xi - 1/6|$ may partially break down during the bouncing regime. When needed, numerical techniques will be employed.

short wavelength limit the effective equation of state obeyed by the relic gravitons is radiative, i.e. $\langle p_{\text{gw}} \rangle = \langle \rho_{\text{gw}} \rangle / 3$ where $\langle p_{\text{gw}} \rangle$ and $\langle \rho_{\text{gw}} \rangle$ correspond to the averaged pressure and energy densities. In this case, $\langle \rho_{\text{gw}} \rangle \sim a^{-4}$, where $a(\tau)$ is the scale factor. In the long wavelength limit the effective equation of state may depend on the salient features of the background evolution. For instance, during the transition from a quasi-de Sitter stage of expansion to a radiation dominated stage, the modes of long wavelengths are compatible with an effective equation of state $\langle p_{\text{gw}} \rangle = -\langle \rho_{\text{gw}} \rangle / 3$ implying that $\langle \rho_{\text{gw}} \rangle \sim a^{-2}$. In this limit the system behaves, effectively, as a generalized fluid dominated by the spatial gradients of the tensor modes of the geometry.

While the conclusions mentioned in the previous paragraph must rely on specific definitions of the energy and pressure densities of the relic gravitons, it is well known that, in general, it is impossible to assign a localized energy density to the gravitational field [33]. This caveat does not exclude the possibility of adopting consistent frameworks for the analysis of a gravitational energy-momentum pseudo-tensor.

To be more specific, the tensor modes of the geometry can be characterized by a rank-two tensor h_{ij} defined in the three spatial dimensions (that will taken to be flat), i.e.

$$ds^2 = a^2(\tau)[d\tau^2 - (\delta_{ij} + h_{ij})dx^i dx^j], \quad h_i^i = \partial_i h_j^i = 0, \quad (1.1)$$

where δ_{ij} is Kroenker symbol and h_{ij} , being traceless and divergence-less, carries two independent degrees of freedom that correspond to the two polarizations of a gravitational wave in a conformally flat Friedmann-Robertson-Walker (FRW) background³. The simplest way of estimating the impact of the created gravitons on the background dynamics is by computing the lowest-order nonlinear corrections to the Einstein tensor

$$\mathcal{G}_\mu^\nu = R_\mu^\nu - \frac{1}{2}\delta_\mu^\nu R, \quad (1.2)$$

where R_μ^ν and R are, respectively, the Ricci tensor and the Ricci scalar. The nonlinear corrections to the Einstein tensor, will consist, to lowest order, of quadratic combinations of h_{ij} that can be formally expressed as⁴

$$\ell_{\text{P}}^2 \mathcal{T}_\mu^\nu = -\delta_{\text{t}}^{(2)} \mathcal{G}_\mu^\nu, \quad (1.3)$$

where the superscript at the right hand side denotes the second-order fluctuation of the corresponding quantity while the subscript refers to the tensor nature of the fluctuations. This procedure is essentially the one described in [34, 35] and has been re-explored, in a related context, by the

³Since h_{ij} is transverse and traceless, the direction of propagation can be chosen to lie along the third axis and, in this case the two physical polarizations of the graviton will be $h_1^1 = -h_2^2 = h_\oplus$ and $h_1^2 = h_2^1 = h_\otimes$. This will be the nomenclature followed in the present paper.

⁴In the present notations the Planck length will be defined as $\ell_{\text{P}} = \sqrt{8\pi G}$ in units $\hbar = c = 1$. Natural gravitational units $16\pi G = 2\ell_{\text{P}}^2 = 1$ will also be adopted when needed.

authors of Refs. [36, 37] mainly in connection with conventional inflationary models where the Universe is always expanding⁵

In [39] (see also [40]) a complementary perspective was invoked and it was observed that, by perturbing the Einstein-Hilbert action to second order in the amplitude of the tensor modes of the geometry in a Friedmann-Robertson-Walker background, each single polarization of the graviton obeys, up to total derivatives, the action of a minimally coupled scalar degree of freedom

$$\delta_t^{(2)} S = \frac{1}{2} \int d^4x a^2(\tau) \eta^{\alpha\beta} \partial_\alpha h \partial_\beta h, \quad (1.4)$$

where the dimensionless amplitude h has been defined as

$$h = \frac{h_\oplus}{\sqrt{2}\ell_P} = \frac{h_\otimes}{\sqrt{2}\ell_P}. \quad (1.5)$$

Consequently, following [39], a natural ansatz for describing the back-reaction of the created gravitons on the background space-time would be to use, for each single polarization, the energy-momentum tensor of a minimally coupled scalar field. This approach has been exploited, for instance, in [6] and in [17] for estimating the energy and pressure densities of the relic gravitons in a multi-stage Universe. A possible weakness of this second approach is that Eq. (1.4) holds, strictly speaking, in a Friedmann-Robertson-Walker background. In spite of this, it is clearly useful to bear in mind this possibility.

The purpose of the present paper is to scrutinize the dynamical back-reaction effects of the relic gravitons in the extreme situation where the background geometry undergoes a contraction that smoothly evolves, through a bounce, into an expanding phase. This sequence of events takes place, for instance, in pre big-bang models. The bouncing behaviour is related to strong deviations from a radiative Universe. Consequently, short wave fluctuations are expected to modify or even restrict the dynamical range of bouncing models since, in this regime, the effective equation of state of relic gravitons is the one of radiation. For long wavelength fluctuations, the qualitative expectation is more difficult to formulate since, as already mentioned, the effective equation of state is sensitive to the specific features of the background evolution before and after the bounce.

Consider then, as an example, one of the simplest realizations of bouncing dynamics, i.e. the one provided by minimal pre-big bang models where, in the Einstein frame, the Universe first contracts as $a(\tau) \sim \sqrt{-\tau/\tau_1}$ and then expands, in the post-big bang phase, as $a(\tau) \sim \sqrt{\tau/\tau_1}$. An accurate description of the bouncing regime in the region $-\tau_1 < \tau < \tau_1$ may be achieved, for instance, by means of a non-local potentials [41, 42, 43] that depend on the so-called shifted dilaton which is

⁵Recently in [38] the field theoretical formulation of General Relativity was further developed with the purpose of deriving an energy-momentum tensor for the gravitational field. Our approach, in the present context, is more modest since we simply want to compare the dynamical consequences of different possible definitions of the energy-momentum pseudo-tensor of the relic gravitons.

usually introduced in the context of the scale-factor-duality symmetry [10] (or more generally, in the treatment of $O(d, d)$ transformations [44, 45] acting on the background fields of the low-energy string effective action). The features of the regular bouncing solutions discussed in [46, 47] are such that the rôle of the dilaton potential is only crucial in the bouncing region while, away from the bounce (i.e. $|\tau| > \tau_1$) the geometry is driven by the kinetic energy of the dilaton field.

As soon as the tensor modes reach into the super-adiabatic regime, i.e. $k\tau \ll 1$ the effective pressure density of the relic gravitons becomes $\langle p_{\text{gw}} \rangle \simeq \langle \rho_{\text{gw}} \rangle$. Consequently, at least up to the bounce, the energy density of the relic gravitons is not likely to dominate on the energy density of the dilatonic sources since the two components evolve exactly in the same way with the scale factor. While it is plausible that only around the bounce the short wavelength modes become dynamically relevant, it is also clear that the whole qualitative picture should be corroborated by a detailed numerical and analytical treatment.

It will be instructive to conduct the calculation of the dynamical back-reaction within different ansatz for the energy-momentum pseudo-tensor. Then the results will be compared. A byproduct of the present analysis will indeed be that different forms of the energy-momentum pseudo-tensor lead, quantitatively, to the same back-reaction effects.

The present paper is then organized as follows. In Section 2 a class of string inspired bouncing cosmologies will be introduced. Section 3 is devoted to the analysis of the production of relic gravitons and to the different definitions of their energy-momentum pseudo-tensor in the framework of bouncing solutions. Section 4 deals with the analytical estimates of the effective barotropic indices. Section 5 describes the implementation of a self-consistent (iterative) scheme that allows to compute the back-reaction effects of relic gravitons. Section 6 summarizes the main lessons to be drawn from the present analysis and contains also the concluding remarks. Finally, various technical results that are relevant for the present investigation are reported in the appendix.

2 A class of regular curvature bounces

Regular bouncing solutions can be obtained by means of dilaton potentials that respect the scale factor duality symmetry [10]. These potentials do not depend solely upon the dilaton field ϕ but rather upon the so-called shifted dilaton, i.e. $\bar{\phi} = \phi - \log \sqrt{-G_s}$ [41, 42, 43] (see also [49]) where G_s is the determinant of the four-dimensional metric in the string frame and in the cosmic time coordinate.

Therefore the starting point of the present analysis is a generally covariant action supplemented by a non-local dilaton potential [46, 47, 48]. The problem will be directly analyzed in the Einstein frame metric where the dilaton field and the Einstein-Hilbert term are decoupled and the relevant

action is [47]

$$S = \int d^4x \sqrt{-g} \left[-\frac{R}{2\ell_{\text{P}}^2} + \frac{1}{2} g^{\alpha\beta} \partial_\alpha \phi \partial_\beta \phi - W(\bar{\phi}) \right], \quad (2.1)$$

where

$$\begin{aligned} W(\bar{\phi}) &= e^\phi V(e^{-\bar{\phi}}), \\ e^{-\bar{\phi}} &= e^{\phi/2} \int d^4y \left(\sqrt{-g} \sqrt{g^{\alpha\beta} \partial_\alpha \phi \partial_\beta \phi} \right)_y \delta(\phi(x) - \phi(y)). \end{aligned} \quad (2.2)$$

In the following the prime denotes a derivation of the corresponding function with respect to his own argument (so, for instance, V' will denote a derivation of V with respect to $e^{-\bar{\phi}}$ and so on).

The evolution equations derived from the action (2.1) are then [47]

$$\mathcal{G}_\mu^\nu = \ell_{\text{P}}^2 [T_\mu^\nu(\phi) + \tilde{T}_\mu^\nu(\phi, g)], \quad (2.3)$$

$$g^{\alpha\beta} \nabla_\alpha \nabla_\beta \phi + e^\phi \left[V - \frac{1}{2} \frac{\partial V}{\partial \bar{\phi}} - e^{\phi/2} \left(\frac{\gamma^{\mu\nu} \nabla_\mu \nabla_\nu \phi}{\sqrt{g^{\alpha\beta} \partial_\alpha \phi \partial_\beta \phi}} \mathcal{I}_1 - V' \mathcal{I}_2 \right) \right] = 0, \quad (2.4)$$

where \mathcal{G}_μ^ν is the Einstein tensor already introduced in Eq. (1.2). In Eq. (2.3) $T_\mu^\nu(\phi)$ and $\tilde{T}_\mu^\nu(\phi, g)$ are, respectively,

$$T_\mu^\nu(\phi) = \partial_\mu \phi \partial^\nu \phi - \frac{1}{2} \delta_\mu^\nu g^{\alpha\beta} \partial_\alpha \phi \partial_\beta \phi, \quad (2.5)$$

$$\tilde{T}_\mu^\nu(\phi, g) = e^\phi \left(V \delta_\mu^\nu + \gamma_\mu^\nu \sqrt{g^{\alpha\beta} \partial_\alpha \phi \partial_\beta \phi} e^{\phi/2} \mathcal{I}_1 \right); \quad (2.6)$$

where the induced metric $\gamma_{\mu\nu}$

$$\gamma_{\mu\nu} = g_{\mu\nu} - \frac{\partial_\mu \phi \partial_\nu \phi}{g^{\alpha\beta} \partial_\alpha \phi \partial_\beta \phi}, \quad (2.7)$$

has been defined. In Eqs. (2.4) and (2.6) the two integrals \mathcal{I}_1 and \mathcal{I}_2 are:

$$\begin{aligned} \mathcal{I}_1(x) &= \frac{1}{\ell_{\text{P}}^3} \int d^4y \left(\sqrt{-g} V' \right)_y \delta(\phi(x) - \phi(y)), \\ \mathcal{I}_2(x) &= \frac{1}{\ell_{\text{P}}^3} \int d^4y \left(\sqrt{-g} \sqrt{g^{\alpha\beta} \partial_\alpha \phi \partial_\beta \phi} \right)_y \delta'(\phi(x) - \phi(y)). \end{aligned} \quad (2.8)$$

Equations (2.3) and (2.4) can now be written for the case of a four-dimensional background geometry characterized by a conformally flat Friedmann-Robertson-Walker metric and by a homogeneous dilaton field:

$$g_{\mu\nu} = a^2(\tau) \eta_{\mu\nu}, \quad \phi = \phi(\tau). \quad (2.9)$$

Using Eq. (2.9), the set of homogeneous equations stemming from Eqs. (2.3) and (2.4) can be linearly combined and the relevant set of evolution equations, in units $2\ell_{\text{P}}^2 = 1$, becomes

$$\mathcal{H}^2 = \frac{\phi'^2}{12} + \frac{e^\phi a^2}{6} V, \quad (2.10)$$

$$\mathcal{H}' = -\frac{\phi'^2}{6} + \frac{a^2 e^\phi}{6} \left[V - \frac{3}{2} \frac{\partial V}{\partial \phi} \right], \quad (2.11)$$

$$\phi'' + 2\mathcal{H}\phi' = -e^\phi a^2 \left[V - \frac{1}{2} \frac{\partial V}{\partial \phi} \right], \quad (2.12)$$

where the prime will denote, from now on, a derivation with respect to the conformal time coordinate τ and $\mathcal{H} = a'/a$.

By summing \mathcal{H}' (from Eq. (2.11)) to $2\mathcal{H}^2$ (from Eq. (2.10)), the right hand side of the obtained equation reconstructs, up to a numerical coefficient, the right hand side of Eq. (2.12) so that the dependence on the potential terms may be eliminated. The remaining equation becomes then particularly simple:

$$\frac{d}{d\tau} \left[a^2 \left(\mathcal{H} + \frac{\phi'}{2} \right) \right] = 0. \quad (2.13)$$

Direct integration of Eq. (2.13) gives then:

$$\mathcal{H} + \frac{\phi'}{2} = \frac{\epsilon}{a^2}, \quad (2.14)$$

where ϵ is the integration constant. Unfortunately, in the conformal time coordinate the integration cannot proceed further with analytical methods. However, Eq. (2.14) can indeed be integrated analytically by defining the new time coordinate σ , i.e.

$$d\sigma = \frac{d\tau}{a^2(\tau)}. \quad (2.15)$$

Since the relation of τ to cosmic time is $dt = a(\tau)d\tau$, the relation of the cosmic time t to the σ -parametrization is simply $dt = a^3(\sigma)d\sigma$. Equation (2.15) can then be used into Eq. (2.14) and the result is

$$\mathcal{F} + \frac{d\phi}{d\sigma} = \epsilon, \quad (2.16)$$

where $\mathcal{F} = (\ln a)_{,\sigma}$ and its relation to \mathcal{H} is simply $\mathcal{H} = \mathcal{F}/a^2$. By integrating once Eq. (2.16) and by naming as σ_1 the new integration constant the following explicit relation between the scale factor and the dilaton field can be obtained

$$a(\sigma) e^{\phi(\sigma)/2} = e^{\epsilon(\sigma+\sigma_1)}. \quad (2.17)$$

Equation (2.17) simply fixes a relationship between $a(\sigma)$ and $\phi(\sigma)$; such a relationship must hold for any potential. Conversely, the particular form of the dilaton potential plays a crucial rôle in determining the relative evolution of the scale factor and of the dilaton whose combination appears directly in Eq. (2.17). Finally, once the potential is chosen, the Hamiltonian constraint of Eq. (2.10) selects the specific value of ϵ .

To proceed even further it is necessary to write Eqs. (2.10), (2.11) and (2.12) in the parametrization defined by Eq. (2.15); in doing so it is useful to notice that

$$\mathcal{H} \rightarrow \frac{\mathcal{F}}{a^2}, \quad \mathcal{H}' \rightarrow \frac{1}{a^2} \left(\frac{d\mathcal{F}}{d\sigma} - 2\mathcal{F}^2 \right). \quad (2.18)$$

Consequently, Eqs. (2.10), (2.11) and (2.12) can be written as

$$\mathcal{F}^2 = \frac{\xi^2}{12} + \frac{e^\phi a^6}{6} V. \quad (2.19)$$

$$\frac{d\mathcal{F}}{d\sigma} = \frac{e^\phi a^6}{2} \left[V - \frac{1}{2} \frac{\partial V}{\partial \bar{\phi}} \right], \quad (2.20)$$

$$\frac{d\xi}{d\sigma} = -e^\phi a^6 \left[V - \frac{1}{2} \frac{\partial V}{\partial \bar{\phi}} \right], \quad (2.21)$$

where $\xi = d\phi/d\sigma$. Equations (2.19) and (2.21) stem directly from Eq. (2.10) and (2.12) by using Eqs. (2.18). Equation (2.20) follows from Eq. (2.11) by eliminating, in the obtained expression, the dependence on \mathcal{F}^2 through Eq. (2.19).

The solutions of the system formed by Eqs. (2.19), (2.20) and (2.21) can now be derived for the general class of potentials $V = -V_0 e^{\alpha \bar{\phi}}$. In this case we have

$$\begin{aligned} a^6 e^\phi V &= -V_0 a^6 e^{\phi + \alpha \bar{\phi}} = -V_0 \frac{e^{-(\alpha-2)\phi/2}}{a^{3(\alpha-2)}}, \\ a^6 e^\phi \left[V - \frac{1}{2} \frac{\partial V}{\partial \bar{\phi}} \right] &= \frac{\alpha-2}{2} V_0 \frac{e^{-(\alpha-2)\phi/2}}{a^{3(\alpha-2)}}, \end{aligned} \quad (2.22)$$

where we used that $\bar{\phi} = \phi - 3 \ln a_s$, $a_s(\tau)$ being the scale factor in the string frame metric. Furthermore bearing in mind that the scale factor in the Einstein frame is given by $a = e^{\phi/2} a_s$, Eqs. (2.22) follow immediately from the definition of the potential in terms of $\bar{\phi}$.

Equations (2.19) and (2.20) can now be combined and the result is

$$\frac{d\mathcal{F}}{d\sigma} + \frac{3}{2}(\alpha-2)\mathcal{F}^2 = \frac{\alpha-2}{8}\xi^2. \quad (2.23)$$

On the other hand, Eq. (2.14) allows to express ξ in terms of ϵ and \mathcal{F} , i.e.

$$\frac{\xi}{2} = \epsilon - \mathcal{F}. \quad (2.24)$$

Eliminating ξ from Eq. (2.23) through Eq. (2.24) the whole problem can be reduced to the following equation

$$\frac{d\mathcal{F}}{d\sigma} = \frac{\alpha-2}{2} [\epsilon^2 - 2\mathcal{F}^2 - 2\epsilon\mathcal{F}], \quad (2.25)$$

that can be easily integrated with the result that \mathcal{F} is

$$\mathcal{F} = -\frac{\epsilon}{2} + \frac{\sqrt{3}}{2} \epsilon \tanh \left[\frac{\beta(\sigma + \sigma_2)}{2} \right], \quad (2.26)$$

where $\beta = \sqrt{3} \epsilon (\alpha - 2)$ and σ_2 is an integration constant. Inserting Eq. (2.26) into Eq. (2.24), the explicit form of ξ turns out to be

$$\xi = 3\epsilon - \sqrt{3} \epsilon \tanh \left[\frac{\beta(\sigma + \sigma_2)}{2} \right]. \quad (2.27)$$

Equations (2.26) and (2.27) can be integrated again so that the explicit functional dependence of the dilaton and of the scale factor upon the time coordinate σ becomes:

$$a(\sigma) = e^{-\phi_b/2} e^{-\frac{\epsilon(\sigma-2\sigma_1)}{2}} \left[\cosh \frac{\beta(\sigma + \sigma_2)}{2} \right]^{\frac{1}{\alpha-2}}, \quad (2.28)$$

$$\phi(\sigma) = \phi_b + 3\epsilon\sigma - \frac{2}{\alpha-2} \ln \cosh \frac{\beta(\sigma + \sigma_2)}{2}. \quad (2.29)$$

The consistency of Eqs. (2.28) and (2.29) with the Hamiltonian constraint (2.19) demands that the value of ϵ is fixed as:

$$3\epsilon^2 = V_0 e^{(\alpha-2)\phi_b} e^{-3(\alpha-2)\sigma_1}. \quad (2.30)$$

Equation (2.28) can now be inserted into Eq. (2.27) to obtain the asymptotic relation (i.e. for $\sigma \rightarrow \pm\infty$) between the σ and τ . This relation is logarithmic in the sense that, up to numerical factors $\sigma \simeq -\ln(-\tau)$ (for σ and τ going to $-\infty$) and $\sigma \simeq \ln \tau$ (for σ and τ going to $+\infty$). This is particularly appropriate for numerical purposes since, in practice, the σ -parametrization acts as a logarithmic scale in the asymptotic regions. On the contrary, the central region of the dynamics (i.e. $\sigma \simeq \sigma_2$) is described by a linear time-scale.

To describe the features of the obtained solution let us fix, for simplicity, $\sigma_1 = \sigma_2 = 0$. In short the basic feature of the solution are the following:

- for $\alpha > 2$ the solution (2.28) and (2.29) describes a smooth interpolation between a contracting regime (i.e. $\mathcal{F} < 0$) for $\sigma < 0$ and an expanding solution, i.e. $\mathcal{F} > 0$ valid for $\sigma > 0$;
- for $\alpha < 2$ the dynamical sequence is reversed since the scale factor expands for $\sigma < 0$ and contracts for $\sigma > 0$, as is can be argued from the specific form of \mathcal{F} (see Eq. (2.26));
- for $\alpha = 2$ the solution always contract and the bouncing behaviour is not realized.

If σ_1 or σ_2 (or both) are different from zero the solutions are not centered around $\sigma = 0$ and the same discussion applies for an appropriately translated coordinate system.

Concerning the third item of the above list, it is interesting to notice that, in the case $\alpha = 2$, the explicit solution reads

$$a(\sigma) = e^{-\phi_b/2} e^{-\epsilon\sigma/2}, \quad \phi(\sigma) = 3\epsilon\sigma + \phi_b, \quad 3\epsilon^2 = V_0, \quad (2.31)$$

implying that $\mathcal{F} = -\epsilon/2$. In Fig. 1 (left panel) the evolution of $\xi(\sigma)$ and $\mathcal{F}(\sigma)$ is illustrated as it emerges from Eqs. (2.26) and (2.27). The time scale is given in terms of $\sigma_b = 1/\epsilon$, i.e. the typical bouncing time. In the left plot, the logarithm⁶ (to base 10) of the scale factor is illustrated for

⁶In the present paper the natural logarithm will always be denoted as \ln while the logarithm to base 10 will be denoted as \log .

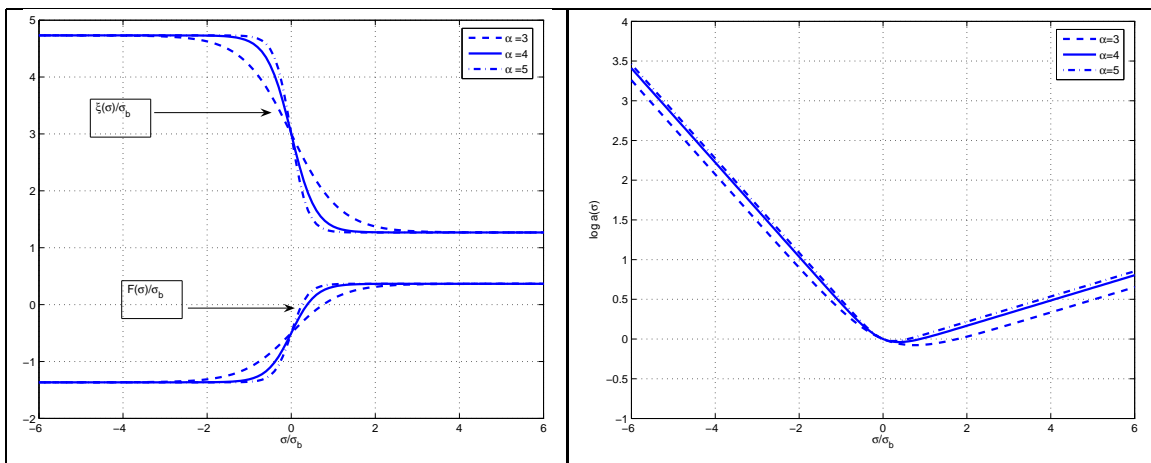


Figure 1: In the left plot the evolution of \mathcal{F}/σ_b and ξ/σ_b are illustrated for different values of the parameter α . In the right plot the logarithm (to base 10) of the scale factor is illustrated for different values of α .

the same range of α . The initial conditions for the solutions can be characterized in terms of ϕ or more precisely $e^{\phi/2}$ that measures the initial strength of the gauge coupling. We shall be primarily interested in the case when the solution contracts for $\sigma < 0$ and expands for $\sigma > 0$ (i.e. $\alpha > 2$). In this situation the pre-big bang initial conditions will be reproduced since $e^{\phi/2} \ll 1$ for $\sigma \rightarrow -\infty$. Notice that ϕ_b measures the strength of the gauge coupling around the bounce, i.e. for $\sigma \simeq 0$. Of particular interest will be the case when $\phi_b \simeq 0$, i.e. when strong coupling is reached just at the bounce. It is clearly always possible to tune ϕ_b in such a way that the gauge coupling is much smaller than 1 but we shall try to avoid this tuning and examine the more realistic situation where $\phi_b \simeq 0$.

The σ -parametrization is particularly useful for the numerical evolution of the fluctuations and for the self-consistent treatment of the dynamical back-reaction effects. It is sometimes practical, in a complementary perspective, to solve for the mode functions directly in the conformal time parametrization. As already remarked, in the conformal time parametrization we cannot rely on exact solutions. Therefore the idea will be to map the asymptotic solutions in the σ parametrization into asymptotic solutions in the τ parametrization and then solve numerically Eqs. (2.10), (2.11) and (2.12). It is therefore necessary to develop the numerical intuition for the evolution of the background in the conformal time parametrization. Of particular technical relevance is the precise mapping of the initial conditions from the σ -parametrization to the conformal time coordinate.

To fix the ideas, consider the case $\alpha = 4$ with the bounce occurs around $\sigma_1 = \sigma_2 = 0$. In this case the mapping of the initial conditions between the σ and the τ parametrization can be derived

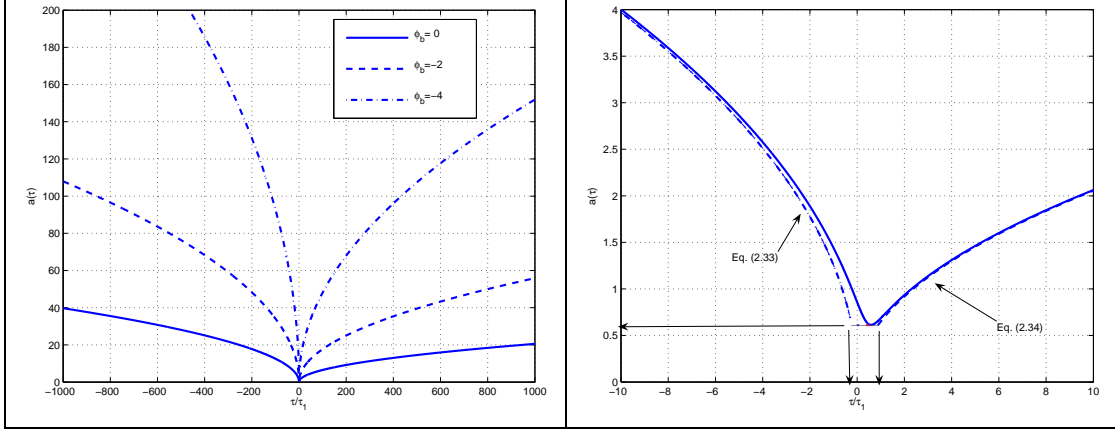


Figure 2: The evolution of the scale factor (left panel) is illustrated for different initial values of the gauge coupling. In the right plot the analytical approximations for the evolution of the scale factor (dashed lines) are compared with the numerical solution.

from the following chain of relations

$$3\epsilon^2 = V_0 e^{2\phi_b} = \frac{e^{-2\phi_b}}{\tau_1^2}, \quad (2.32)$$

where the first equality is nothing but Eq. (2.30) in the case $\alpha = 4$ (and $\sigma_1 = 0$). The second equality is fixed by solving directly the Hamiltonian constraint of Eq. (2.10) in the asymptotic regions (i.e. $\tau \rightarrow \pm\infty$). Equation (2.32) fixes the relation between the bouncing time in the σ -parametrization, i.e. $\sigma_b = 1/\epsilon$, in terms of the bouncing time in the τ -parametrization, i.e. τ_1 . In Fig. 2 the numerical integration of Eqs. (2.10), (2.11) and (2.12) is illustrated in terms of the scale factor. In particular, for $\tau < -\tau_1$ the solution is well approximated by

$$a(\tau) = a_- \sqrt{\frac{-\tau}{2\tau_1}}, \quad a_- = e^{-\phi_b/2} \sqrt{\frac{2(\sqrt{3}+1)}{\sqrt{3}}}, \quad (2.33)$$

while for $\tau > -\tau_1$ the solution is well approximated by

$$a(\tau) = a_+ \sqrt{\frac{\tau}{2\tau_1}}, \quad a_+ = e^{-\phi_b/2} \sqrt{\frac{2(\sqrt{3}-1)}{\sqrt{3}}}, \quad (2.34)$$

where ϕ_b is the same constant introduced in Eq. (2.29). In the pre-bounce region the evolution of the dilaton can be obtained from Eq. (2.29) by using the asymptotic relation between τ and σ in the limit $\tau \rightarrow -\infty$ and $\sigma \rightarrow -\infty$. The result is:

$$\phi(\tau) = \phi_b - (\sqrt{3}-1) \ln 2 - \sqrt{3} \ln \left(\frac{\sqrt{3}+1}{\sqrt{3}} \right) - \sqrt{3} \ln \left(-\frac{\tau}{\tau_1} \right). \quad (2.35)$$

In the intermediate region, the minimum of the scale factor corresponds to

$$a_{\min} = 0.61 e^{-\phi_b/2}. \quad (2.36)$$

The “width” of the bounce is illustrated in Fig. 2 (right plot) and can be estimated analytically as

$$\frac{\tau_-}{\tau_1} = -\frac{0.74}{a_-^2} e^{-\phi_b}, \quad \frac{\tau_+}{\tau_1} = \frac{0.74}{a_+^2} e^{-\phi_b}. \quad (2.37)$$

In Fig. 2 the values of τ_{\pm} correspond to the two vertical arrows around the origin.

By changing the various parameters it appears that both $a^2 H^2$ and $\phi'^2/2$ are not sensitive to the value of ϕ_b but rather they depend on τ_1 . In particular, it turns out that

$$\mathcal{H}^2 \simeq \frac{0.61}{\tau_1^2}, \quad \frac{\phi'^2}{2} \simeq \frac{7.5}{\tau_1^2}. \quad (2.38)$$

In the case $\alpha = 2$ the solution can be expressed exactly also in the conformal time parametrization. Recalling Eq. (2.15) we obtain that

$$\sigma = -\frac{1}{\epsilon} \ln(-\epsilon)\tau, \quad a(\tau) = e^{-\phi_b/2} \sqrt{-\epsilon\tau}, \quad \phi(\tau) = \phi_b - 3 \ln(-\epsilon\tau). \quad (2.39)$$

Thus, unlike the case $\alpha > 3$ the solution with $\alpha = 2$ is singular in the conformal time parametrization.

The σ parametrization has one more important feature that has been already implicitly treated in Eq. (2.18). While the sign of \mathcal{H} and \mathcal{F} is preserved by the mapping $\tau \rightarrow \sigma$, the sign of \mathcal{H}' is, in general, different from the sign of $\mathcal{F}_{,\sigma}$. The simplest way of realizing this aspect is to notice that, from Eqs. (2.15) and (2.18) we can write

$$\mathcal{F} = a^2 \mathcal{H}, \quad \frac{\partial \mathcal{F}}{\partial \sigma} = a^4 (\mathcal{H}' + 2\mathcal{H}^2). \quad (2.40)$$

Consider now the simple case of a radiation-dominated Universe. In this case $a(\tau) = (\tau + 2\tau_1)/\tau_1$ for $\tau \geq -\tau_1$. Consequently, from Eq. (2.40), \mathcal{H} and \mathcal{F} will have the same sign but $\mathcal{F}_{,\sigma}$ will be always positive while $\mathcal{H}' = -1/(\tau + 2\tau_1)^2$ will always be negative. The cure for this type of problem is very simple. The invariant quantities (like for instance) the Ricci scalar are always the same in both coordinate systems. So, for instance, in a radiation dominated Universe the background Ricci scalar, i.e. \bar{R} is always zero both in the τ and in the σ parametrizations. In fact,

$$\bar{R} = -\frac{6}{a^2} (\mathcal{H}^2 + \mathcal{H}') = -\frac{6}{a^6} \left(\frac{\partial \mathcal{F}}{\partial \sigma} - \mathcal{F}^2 \right), \quad (2.41)$$

where the second equality follows by using Eq. (2.18). Now, it is easy to show that, for a radiation-dominated Universe, the evolution equation obeyed by \mathcal{F} is exactly $\mathcal{F}_{,\sigma} = \mathcal{F}^2$.

It is appropriate to remark at this point that the bouncing solutions obtained here in the framework of the low-energy string effective action differ from the ones derived in the presence of spatial curvature and in a general relativistic context. For instance in [50, 51] (see also [52, 53] and references therein) spatially closed models driven by a massive scalar were studied. As anticipated, in this framework the dynamical sequence of events differs from the one discussed here. In [50, 51] the Universe first deflates, then bounces and finally inflates ⁷. In spite of this statement, the treatment the dynamical back-reaction of relic gravitons in closed bounces can be developed by following the same methods discussed here.

3 Energy-momentum pseudo-tensor(s)

3.1 General considerations

Recalling Eq. (1.1), the quadratic action for h_{ij} can be obtained by perturbing Eq. (2.1) to second-order in the amplitude of the tensor fluctuations of the metric. Some relevant expressions can be found in the appendix A. Up to total derivatives, the result can be written as

$$\delta_t^{(2)} S = S_{\text{gw}} = \frac{1}{8\ell_{\text{P}}^2} \int d^3x d\tau \sqrt{-\bar{g}} \partial_\alpha h_i^j \partial_\beta h_j^i \bar{g}^{\alpha\beta}, \quad (3.1)$$

where $\bar{g}_{\alpha\beta} = a^2(\tau)\eta_{\alpha\beta}$ and $\eta_{\alpha\beta}$ is the Minkowski metric.

As discussed in connection with Eq. (1.1), the two polarizations of the graviton can be chosen to be $h_1^1 = -h_2^2 = h_\oplus$ and $h_1^2 = h_2^1 = h_\otimes$. Furthermore recalling the notations of Eq. (1.5), Eq. (3.1) becomes, for a single tensor polarization

$$S_{\text{gw}} = \frac{1}{2} \int d^3x d\tau \sqrt{-\bar{g}} \partial_\alpha h \partial_\beta h \bar{g}^{\alpha\beta}, \quad (3.2)$$

Using the parametrization defined in Eq. (2.15), Eq. (3.2) can be also written as

$$S_{\text{gw}} = \frac{1}{2} \int d^3x d\sigma \left[\left(\frac{\partial h}{\partial \sigma} \right)^2 - a^4(\sigma) \partial_m h \partial^m h \right]. \quad (3.3)$$

The associated canonical momentum, i.e. $\Pi = \partial_\sigma h$ allows to obtain the Hamiltonian of the tensor modes, i.e.

$$H_{\text{gw}}(\sigma) = \frac{1}{2} \int d^3x \left[\Pi^2 + a^4 \partial_m h \partial^m h \right]. \quad (3.4)$$

By promoting the classical fields to quantum mechanical operators we have that ⁸

$$\hat{h}(\vec{x}, \sigma) = \frac{1}{2(2\pi)^{3/2}} \int d^3k \left[\hat{h}_{\vec{k}}(\sigma) e^{-i\vec{k}\cdot\vec{x}} + \hat{h}_{\vec{k}}^\dagger(\sigma) e^{i\vec{k}\cdot\vec{x}} \right],$$

⁷This class of closed bounces has a long history. For instance in [54, 55] useful analytical solutions were derived and exploited. In connection with this problem see also [56, 57, 58].

⁸Notice that, within our set of conventions, $\hat{h}_{-\vec{k}}^\dagger = \hat{h}_{\vec{k}}$ and $\hat{\Pi}_{-\vec{k}}^\dagger = \hat{\Pi}_{\vec{k}}$.

$$\hat{\Pi}(\vec{x}, \sigma) = \frac{1}{2(2\pi)^{3/2}} \int d^3k [\hat{\Pi}_{\vec{k}}(\sigma) e^{-i\vec{k}\cdot\vec{x}} + \hat{\Pi}_{\vec{k}}^\dagger(\sigma) e^{i\vec{k}\cdot\vec{x}}]. \quad (3.5)$$

In the Heisenberg representation the evolution of the field operators can be written as

$$\hat{h}_{\vec{k}}(\sigma) = \hat{a}_{\vec{k}}(\sigma_1) F_k(\sigma) + \hat{a}_{-\vec{k}}^\dagger(\sigma_1) F_k(\sigma)^*, \quad (3.6)$$

$$\hat{\Pi}_{\vec{k}}(\sigma) = \hat{a}_{\vec{k}}(\sigma_1) G_k(\sigma) + \hat{a}_{-\vec{k}}^\dagger(\sigma_1) G_k(\sigma)^*, \quad (3.7)$$

where $\hat{a}_{\vec{k}}(\sigma_1)$ and $\hat{a}_{-\vec{k}}(\sigma_1)$ annihilate the vacuum for $\sigma_1 \rightarrow -\infty$. The mode functions F_k and G_k now obey

$$\frac{d^2 F_k}{d\sigma^2} + \Omega^2 F_k = 0, \quad G_k = \frac{dF_k}{d\sigma}, \quad (3.8)$$

where $\Omega = ka^2(\sigma)$.

3.2 Mixing coefficients

In the short wavelength limit, i.e. $k|\tau| > 1$ the mode function $F_k(\sigma)$ has an oscillating behaviour. This regime characterizes the asymptotics of the evolution of the mode functions. Initially, for $\sigma \rightarrow -\infty$ the approximate solution of Eq. (3.8) is simply given by

$$F_k(\sigma) = \frac{1}{\sqrt{2\Omega}} e^{-i \int \Omega d\sigma}, \quad G_k(\sigma) = -\frac{1}{\sqrt{2\Omega}} [\mathcal{F} + i\Omega] e^{-i \int \Omega d\sigma}. \quad (3.9)$$

In the limit $\sigma \rightarrow +\infty$ the solution can be expressed by means of two mixing coefficients $c_+(k)$ and $c_-(k)$, i.e.

$$\begin{aligned} F_k(\sigma) &= \frac{1}{\sqrt{2\Omega}} \left[c_+(k) e^{-i \int \Omega d\sigma} + c_-(k) e^{i \int \Omega d\sigma} \right], \\ G_k(\sigma) &= \frac{1}{\sqrt{2\Omega}} \left[-(\mathcal{F} + i\Omega) c_+(k) e^{-i \int \Omega d\sigma} + (i\Omega - \mathcal{F}) c_-(k) e^{i \int \Omega d\sigma} \right]. \end{aligned} \quad (3.10)$$

In the long wavelength limit, i.e. $k|\tau| < 1$ the approximate solution of Eq. (3.8) across the bounce is even simpler and it is given by

$$F_k = A_k + B_k \sigma, \quad G_k = B_k. \quad (3.11)$$

It is relevant to remark here that the condition $k|\tau| \simeq 1$ reads, in the σ -parametrization,

$$\left| \int \Omega d\sigma \right| \simeq 1. \quad (3.12)$$

Due to the presence of the absolute values, there will be two distinct moments, in the dynamical evolution, where the condition $k|\tau| = 1$ is verified. Before the bounce, i.e. for $\sigma < 0$, for a given mode k the condition $-k\tau(\sigma) \simeq 1$ will define the time of ‘‘exit’’ in the σ parametrization. The notation $\tau(\sigma)$ simply means that the specific relation between τ and σ has to be derived from Eq.

(2.15) by using the appropriate expression of the scale factor. After the bounce, i.e. for $\sigma > 0$, the condition $k\tau(\sigma) \simeq 1$ will define the time of “reentry” in the σ -parametrization.

Defining conventionally the typical time scale of the bounce as $\sigma_b = 1/\epsilon$, consider the expression of the scale factor given in Eq. (2.28). In units of bouncing times the exit and reentry occur, approximately, for

$$\frac{\sigma_{\text{ex}}}{\sigma_b} = -\frac{1}{\sqrt{3}+1} \ln \left[\frac{\sqrt{3}+1}{\kappa} e^{\phi_b} 2^{2/(\alpha-2)} \right], \quad (3.13)$$

$$\frac{\sigma_{\text{re}}}{\sigma_b} = \frac{1}{\sqrt{3}-1} \ln \left[\frac{\sqrt{3}-1}{\kappa} e^{\phi_b} 2^{2/(\alpha-2)} \right], \quad (3.14)$$

where we defined $\kappa = k\sigma_b$, i.e. the wave-number in units of inverse bounce time. Equations (3.13) and (3.14) can be easily derived from Eq. (3.12) by using the explicit expressions of $a(\sigma)$ given in Eq. (2.28) evaluated, respectively, in the limits $\sigma < -\sigma_b$ and $\sigma > \sigma_b$. Equations (3.13) and (3.14) are derived by fixing $\sigma_1 = \sigma_2 = 0$ in Eq. (2.28) and by using Eq. (2.15). Moreover, because of the considerations elaborated in the previous Section, the expressions given in Eqs. (3.13) and (3.14) hold for $\alpha > 2$.

For modes $\kappa < 1$, the three solutions given in Eqs. (3.9), (3.10) and (3.11) can be appropriately matched in such a way that the field operators are continuous function of σ . This procedure leads to the determination of the coefficients A_k, B_k

$$A_k = \frac{1}{\sqrt{2\Omega_{\text{ex}}}} e^{-ik\tau_{\text{ex}}} [1 + (\mathcal{F}_{\text{ex}} + i\Omega_{\text{ex}})\sigma_{\text{ex}}], \quad B_k = -\frac{1}{\sqrt{2\Omega_{\text{ex}}}} e^{-ik\tau_{\text{ex}}} (\mathcal{F}_{\text{ex}} + i\Omega_{\text{ex}}), \quad (3.15)$$

and, ultimately, of the mixing coefficients $c_{\pm}(k)$:

$$c_-(k) = -\frac{i}{2\sqrt{\Omega_{\text{ex}}\Omega_{\text{re}}}} e^{-ik(\tau_{\text{re}}+\tau_{\text{ex}})} [(\mathcal{F}_{\text{re}} - \mathcal{F}_{\text{ex}}) + i(\Omega_{\text{re}} - \Omega_{\text{ex}}) - (\mathcal{F}_{\text{re}} + i\Omega_{\text{re}})(\mathcal{F}_{\text{ex}} + i\Omega_{\text{ex}})(\sigma_{\text{re}} - \sigma_{\text{ex}})], \quad (3.16)$$

$$c_+(k) = -\frac{i}{2\sqrt{\Omega_{\text{ex}}\Omega_{\text{re}}}} e^{-ik(\tau_{\text{ex}}-\tau_{\text{re}})} [(\mathcal{F}_{\text{ex}} - \mathcal{F}_{\text{re}}) + i(\Omega_{\text{re}} + \Omega_{\text{ex}}) + (\mathcal{F}_{\text{re}} - i\Omega_{\text{re}})(\mathcal{F}_{\text{ex}} + i\Omega_{\text{ex}})(\sigma_{\text{re}} - \sigma_{\text{ex}})]. \quad (3.17)$$

In Eqs. (3.15), (3.16) and (3.17), the obvious notations $\Omega_{\text{ex}} = \Omega(\sigma_{\text{ex}})$, $\mathcal{F}_{\text{ex}} = \mathcal{F}(\sigma_{\text{ex}})$ (and similarly for Ω_{re} and \mathcal{F}_{re}) have been employed. Equations (3.16) and (3.17) imply that $|c_+(k)|^2 - |c_-(k)|^2 = 1$ which is a simple consequence of the unitary evolution. For $\kappa > 1$ the mixing coefficient is exponentially suppressed. To assess accurately the form of exponential suppression, a numerical treatment is necessary. The strategy here is to integrate numerically Eqs. (3.8) with initial conditions given by Eq. (3.9) and to obtain, numerically the mixing coefficients, i.e.

$$|c_+(k)|^2 - |c_-(k)|^2 = i[F_k^*(\sigma)G_k(\sigma) - F_k(\sigma)G_k^*(\sigma)], \quad (3.18)$$

$$|c_+(k)|^2 + |c_-(k)|^2 = \frac{1}{\Omega} \{ |G_k(\sigma)|^2 + (\mathcal{F}^2 + \Omega^2) |F_k(\sigma)|^2 + \mathcal{F}[F_k^*(\sigma)G_k(\sigma) + F_k(\sigma)G_k^*(\sigma)] \}. \quad (3.19)$$

For the numerical consistency of the whole approach, it must be true for each specific numerical integration, that the combination reported in Eq. (3.18), corresponding to the Wronskian of the solution, is equal to 1 (since it is chosen to be equal to one at the initial integration time, see Eq. (3.9)). The numerical accuracy of the Wronskian normalization condition is a check of the consistency of the whole approach. Along the same lines, the combination in Eq. (3.19) must go to a constant for $\sigma \rightarrow +\infty$.

A set of first-order equations valid for the mixing coefficients will now be discussed. Defining

$$e_{\pm} = e^{\pm i \int \Omega d\sigma}, \quad (3.20)$$

it is possible to find that the mixing coefficients obey

$$\frac{dc_+}{d\sigma} = \frac{1}{2} \frac{d \ln \Omega}{d\sigma} e_+^2 c_-, \quad \frac{dc_-}{d\sigma} = \frac{1}{2} \frac{d \ln \Omega}{d\sigma} e_-^2 c_+. \quad (3.21)$$

Equation (3.21) was derived, in a related context, in Ref. [16]. Since $c_+(k)$ and $c_-(k)$ are two complex quantities subjected to the condition $|c_+(k)|^2 - |c_-(k)|^2 = 1$, they correspond, overall to three real variables that can be chosen to be

$$\begin{aligned} \bar{n}_k &= |c_-(k)|^2, \\ p_k &= c_+(k)c_-^*(k)e_-^2 + c_-(k)c_+^*(k)e_+^2, \\ q_k &= i[c_+(k)c_-^*(k)e_-^2 - c_+^*(k)c_-(k)e_+^2]. \end{aligned} \quad (3.22)$$

The quantities \bar{n}_k , p_k and q_k obey the following set of equations

$$\frac{d\bar{n}_k}{d\sigma} = \mathcal{F}p_k, \quad (3.23)$$

$$\frac{dp_k}{d\sigma} = 2\mathcal{F}(1 + 2\bar{n}_k) - 2\Omega q_k, \quad (3.24)$$

$$\frac{dq_k}{d\sigma} = 2\Omega p_k. \quad (3.25)$$

The initial conditions should be such that, initially, $c_+(k) = 1$ and $c_- = 0$, i.e.

$$\bar{n}_k(\sigma_i) = 0, \quad p_k(\sigma_i) = 0, \quad q_k(\sigma_i) = 0. \quad (3.26)$$

Now the analytical estimates will be corroborated by numerical integration. One of the pleasant features of the σ - parametrization is that the spectrum of the canonical momenta is strictly constant in the long wavelength limit. The spectrum of canonical momenta is the Fourier transform of the two-point correlation function of $\hat{\Pi}(\vec{x}, \sigma)$, i.e.

$$\langle \hat{\Pi}(\vec{x}, \sigma) \hat{\Pi}(\vec{y}, \sigma) \rangle = \int d \ln k |\delta_{\Pi}(k, \sigma)|^2 \frac{\sin kr}{kr}, \quad (3.27)$$

where

$$|\delta_{\Pi}(k, \sigma)|^2 = \frac{k^3}{2\pi^2} |G_k(\sigma)|^2. \quad (3.28)$$

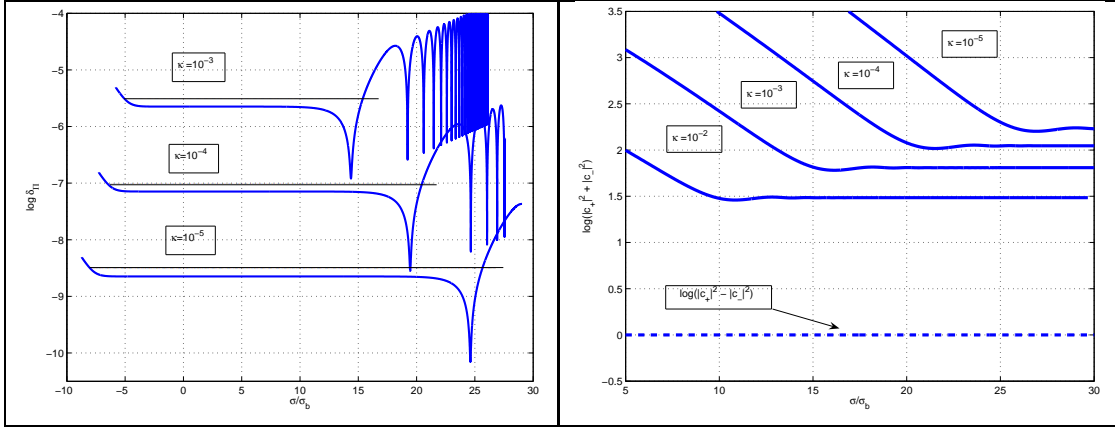


Figure 3: In the plot at the left, the numerical result of the spectrum of the canonical momenta (thick lines), δ_{Π} is compared with the analytical expectation (thin lines) for different values of the wave-numbers. In the right plot, the numerical evaluation of the mixing coefficients reported for $\kappa \ll 1$ (see Eqs. (3.18) and (3.19)). In both plots the logarithm (to base 10) of the corresponding function is illustrated as a function of σ in units of bouncing time σ_b . The background used for this integration corresponds to the case $\alpha = 4$, $\phi_b = 0$ and $\sigma_1 = \sigma_2 = 0$.

Equations (3.27) and (3.28) can be obtained by using Eqs. (3.5) together with Eqs. (3.6) and (3.7). When performing the appropriate quantum mechanical expectation values (in the Heisenberg representation) it should be recalled that $\langle \hat{a}_{\vec{k}} \hat{a}_{\vec{p}}^\dagger \rangle = \delta^{(3)}(\vec{k} - \vec{p})$.

Consequently, from Eq. (3.11) and from the second relation reported in Eq. (3.15) we get

$$\delta_{\Pi}(k, \sigma) = \frac{k^{3/2}}{2\pi} \sqrt{\frac{\mathcal{F}_{\text{ex}}^2 + \Omega_{\text{ex}}^2}{\Omega_{\text{ex}}}}, \quad (3.29)$$

where the quantities at the right hand side are fully determined analytically by using Eqs. (3.13) and (3.15) and by recalling Eq. (2.26). In Fig. 3 (left panel), the analytical expectation given by Eq. (3.29) is compared with the numerical result obtained by integrating Eqs. (3.8) with initial conditions dictated by Eq. (3.10). In Fig. 3 (plot at the right) the numerical result for the integration of Eqs. (3.8) with initial conditions dictated by Eq. (3.10) is reported in terms of the mixing coefficients. We checked that, within the accuracy of the algorithm, the system of Eqs. (3.23), (3.24) and (3.25) with initial conditions given by Eq. (3.26) reproduces the same asymptotic results for the mixing coefficients. From the analytical estimate the spectrum of the mixing coefficients, in the limit $\sigma \gg \sigma_b$, leads to

$$|c_+(k)|^2 + |c_-(k)|^2 \simeq \frac{11}{4} + \frac{25}{16} \ln^2 \kappa \quad (3.30)$$

that agrees with the explicit numerical calculation of the same quantity reported in Fig. 3. This

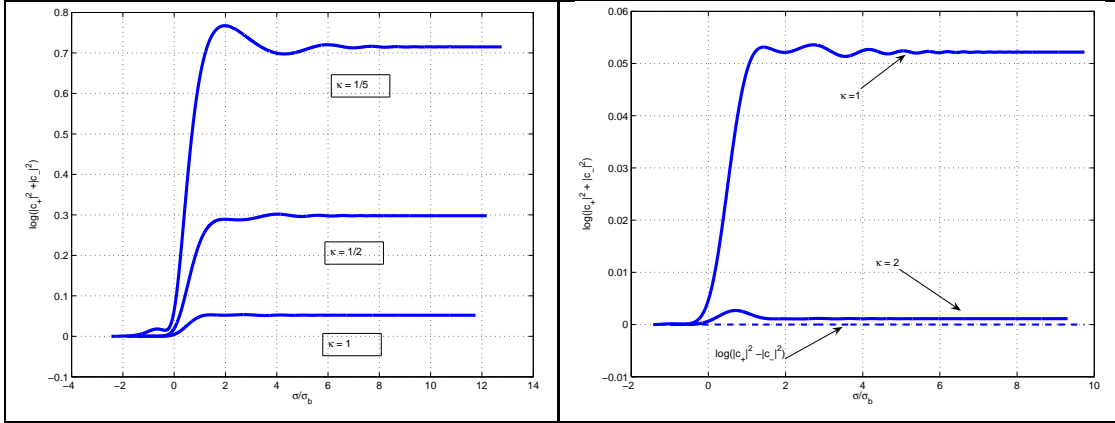


Figure 4: The suppression of the mixing coefficients is illustrated for the regime $\kappa > 1$. It is clear from both plots that when κ increases from $\kappa \leq 1$ to $\kappa > 1$, $|c_-(k)|^2 \rightarrow 0$. The background parameters are the same as in Fig. 3.

statement can be explicitly verified by inserting different values of κ and by comparing the obtained results with numerical values illustrated in the right plot of Fig. 3. For instance, for $\kappa = 10^{-2}$ we get, from Eq. (3.30), $\log[|c_+(k)|^2 + |c_-(k)|^2] \simeq 1.55$, for $\kappa \sim 10^{-5}$ we get $\log[|c_+(k)|^2 + |c_-(k)|^2] \simeq 2.13$ and so on.

While the right plot of Fig. 3 nicely illustrates the case $\kappa \ll 1$, Fig. 4 deals with the case $\kappa \simeq 1$. In this regime, the mixing coefficient $c_-(k)$ is known to be exponentially suppressed. It is clear that from the plot at the right that as κ approaches 1 the mixing is suppressed in such a way that for $\kappa \sim 1$ we have that $(|c_+(k)|^2 + |c_-(k)|^2) \simeq (|c_+(k)|^2 - |c_-(k)|^2)$ implying that $|c_-(k)|^2 \simeq 0$.

A relevant implication of the results reported so far is that since the spectrum of the mixing coefficients is logarithmically increasing with the wave-number (for $\kappa = k\sigma_b < 1$), the spectra of the field operators i.e. $\delta_h \simeq k^{3/2}|F_k(\sigma)|$ (related to the Fourier transform of the two-point function at equal times) will be violet (up to logarithmic corrections). By parametrizing the spectrum as $\delta_h \simeq k^{(n_t-1)/2}$ we have, in the example discussed so far, $n_t = 4$ (up to logarithmic corrections). Moreover, since the spectrum of the mixing coefficients increases with frequency it is plausible to expect that the energy spectrum will be even steeper as a function of the wave-number k . Consequently, the energy spectrum will be convergent in the infrared. In the ultraviolet, the maximally amplified κ , i.e. $\kappa \sim 1$ will give a natural ultraviolet cut-off of the energy density when the (initial) zero-point energy is appropriately subtracted.

3.3 Energy and pressure densities of relic gravitons

Different possibilities for assigning the energy and pressure densities of the relic gravitons will now be examined. The first strategy is to compute the second-order corrections to the Einstein tensor \mathcal{G}'_μ that appears in Eq. (2.3). The details of the calculation are reported in the appendix and the main result for the components of the energy-momentum pseudo-tensor can be expressed, in the conformal time parametrization, as follows:

$$\mathcal{T}_0^0 = \frac{1}{a^2 \ell_{\text{P}}^2} \left[\mathcal{H} h'_{k\ell} h^{k\ell} + \frac{1}{8} (\partial_m h_{k\ell} \partial^m h^{k\ell} + h'_{k\ell} h^{k\ell'}) \right], \quad (3.31)$$

$$\mathcal{T}_i^j = \frac{\mathcal{T}}{3} \delta_i^j + \Sigma_i^j, \quad (3.32)$$

where

$$\mathcal{T} = \frac{1}{a^2 \ell_{\text{P}}^2} \left[\frac{5}{8} h'_{k\ell} h^{k\ell'} - \frac{7}{8} \partial_m h_{k\ell} \partial^m h^{k\ell} \right], \quad (3.33)$$

$$\begin{aligned} \Sigma_i^j = \frac{1}{a^2 \ell_{\text{P}}^2} \left\{ \frac{1}{6} \left[h'_{k\ell} h^{k\ell'} - \frac{1}{2} \partial_m h_{k\ell} \partial^m h^{k\ell} \right] \delta_i^j + \frac{1}{2} \partial_m h_{\ell i} \partial^m h^{\ell j} - \frac{1}{4} \partial_i h_{k\ell} \partial^j h^{k\ell} \right. \\ \left. - \frac{1}{2} h'_{ki} h^{kj'} \right\}, \end{aligned} \quad (3.34)$$

with $\Sigma_i^i = 0$. From Eqs. (3.31) and (3.33) the components of the energy and pressure density can be easily obtained since, by definition, $\rho_{\text{gw}} = \mathcal{T}_0^0$ and $p_{\text{gw}} = -\mathcal{T}/3$.

The components of the energy-momentum pseudo-tensor given in Eqs. (3.31) and (3.32) are not covariantly conserved. However, since the Bianchi identity $\nabla_\mu \mathcal{G}'^\mu_\nu = 0$ should be valid to all orders, we will also have that:

$$\delta_t^{(2)} (\nabla_\mu \mathcal{G}'^\mu_\nu) = 0, \quad (3.35)$$

whose explicit form is

$$\begin{aligned} \partial_\mu \delta_t^{(2)} \mathcal{G}'^\mu_\nu + \delta_t^{(2)} \Gamma_{\mu\alpha}^\mu \bar{\mathcal{G}}'_\nu^\alpha + \bar{\Gamma}_{\mu\alpha}^\mu \delta_t^{(2)} \mathcal{G}'^\alpha_\nu + \delta_t^{(1)} \Gamma_{\mu\alpha}^\mu \delta_t^{(1)} \mathcal{G}'^\alpha_\nu \\ - \delta_t^{(2)} \Gamma_{\nu\alpha}^\beta \bar{\mathcal{G}}'_\beta^\alpha - \bar{\Gamma}_{\nu\alpha}^\beta \delta_t^{(2)} \mathcal{G}'^\alpha_\beta - \delta_t^{(1)} \Gamma_{\nu\alpha}^\beta \delta_t^{(1)} \mathcal{G}'^\alpha_\beta = 0. \end{aligned} \quad (3.36)$$

Recalling now the components of the energy-momentum pseudo-tensor and the results for the fluctuations of the Christoffel symbols (i.e. Eqs. (A.3) of the appendix) we have

$$\frac{\partial \rho_{\text{gw}}}{\partial \tau} + 3\mathcal{H}(\rho_{\text{gw}} + p_{\text{gw}}) - \frac{2(\mathcal{H}^2 - \mathcal{H}')}{a^2 \ell_{\text{P}}^2} \delta_t^{(2)} \Gamma_{k0}^k = 0, \quad (3.37)$$

that can also be written as

$$\frac{\partial \rho_{\text{gw}}}{\partial \tau} + 3\mathcal{H}(\rho_{\text{gw}} + \mathcal{P}_{\text{gw}}) = 0 \quad (3.38)$$

where

$$\mathcal{P}_{\text{gw}} = p_{\text{gw}} + \frac{(\mathcal{H}^2 - \mathcal{H}')}{3\mathcal{H}a^2} h'_{k\ell} h^{k\ell}. \quad (3.39)$$

Equations (3.31), (3.33) and (3.39) imply that the operators corresponding to the energy and pressure densities are, in the σ -parametrization,

$$\hat{\rho}_{\text{gw}} = \frac{1}{a^6} \left\{ 4\mathcal{F}[\hat{h}\hat{\Pi} + \hat{\Pi}\hat{h}] + a^4 \partial_m \hat{h} \partial^m \hat{h} + \hat{\Pi}^2 \right\}, \quad (3.40)$$

$$\hat{p}_{\text{gw}} = \frac{1}{3a^6} \left[-5\hat{\Pi}^2 + 7a^4 (\partial_m \hat{h})(\partial^m \hat{h}) \right], \quad (3.41)$$

$$\hat{\mathcal{P}}_{\text{gw}} = \hat{p}_{\text{gw}} + \frac{4}{3a^6} \left(\mathcal{F} - \frac{d \ln \mathcal{F}}{d\sigma} \right) [\hat{\Pi}\hat{h} + \hat{h}\hat{\Pi}], \quad (3.42)$$

where \hat{h} and $\hat{\Pi}$ are the canonical field operators defined in Eq. (3.5). The averaged components of the energy-momentum pseudo-tensor can be obtained by taking the expectation values of the operators defined in Eqs. (3.40), (3.41) and (3.42) and by recalling that the initial state is the one annihilated by the creation and destruction operators of Eqs. (3.6) and (3.7). The result is then expressed in terms of the appropriate mode functions, i.e.

$$\langle \hat{\rho}_{\text{gw}} \rangle = \frac{1}{a^6} \int \frac{d^3 k}{(2\pi)^3} \left\{ 4\mathcal{F}[F_k(\sigma)G_k^*(\sigma) + F_k^*(\sigma)G_k(\sigma)] + \Omega^2 |F_k(\sigma)|^2 + |G_k(\sigma)|^2 \right\}, \quad (3.43)$$

$$\langle \hat{p}_{\text{gw}} \rangle = \frac{1}{3a^6} \int \frac{d^3 k}{(2\pi)^3} [7\Omega^2 |F_k(\sigma)|^2 - 5|G_k(\sigma)|^2], \quad (3.44)$$

$$\langle \hat{\mathcal{P}}_{\text{gw}} \rangle = \langle \hat{p}_{\text{gw}} \rangle + \frac{4}{3a^6} \int \frac{d^3 k}{(2\pi)^3} \left(3\mathcal{F} - \frac{d \ln \mathcal{F}}{d\sigma} \right) [F_k(\sigma)G_k^*(\sigma) + F_k^*(\sigma)G_k(\sigma)]. \quad (3.45)$$

It is relevant to remark here that Eq. (3.8) implies that $\partial_\sigma \langle \hat{\rho}_{\text{gw}} \rangle + 3\mathcal{F} \langle \hat{\rho}_{\text{gw}} + \hat{\mathcal{P}}_{\text{gw}} \rangle = 0$. The initial conditions for the field operators (3.6) and (3.7) for $\sigma_i \rightarrow -\infty$ imply that the contribution of the zero-point energy is given by $\int (k^4)/(2\pi^2 a^4) d \ln k$ (where we recalled that $\Omega = k a^2$). To discard this quantity by appropriate subtraction (both in the energy and pressure densities) amounts to neglect the contribution of the zero-point oscillations of the vacuum. As already mentioned, there are different ansatz for the energy-momentum pseudo-tensor that have been proposed in order to treat back-reaction effects of the relic gravitons. It is therefore appropriate to comment here about these possibilities. By looking at the form of Eq. (3.2), the authors of Ref. [39] (see also [40]) argued that a natural ansatz for the energy and pressure densities of the relic gravitons is the one we can derive from the energy-momentum tensor of a minimally coupled scalar field for each of the two tensor polarizations. This consideration implies that the energy and pressure densities can be written as

$$\hat{\rho}_{\text{gw}} = \frac{1}{a^6} [\hat{\Pi}^2 + a^4 \partial_m \hat{h} \partial^m \hat{h}], \quad (3.46)$$

$$\hat{p}_{\text{gw}} = \frac{1}{a^6} \left[\hat{\Pi}^2 - \frac{a^4}{3} \partial_m \hat{h} \partial^m \hat{h} \right]. \quad (3.47)$$

The averaged energy and pressure densities become then:

$$\langle \hat{\rho}_{\text{gw}} \rangle = \frac{1}{a^6} \int \frac{d^3 k}{(2\pi)^3} [|G_k(\sigma)|^2 + \Omega^2 |F_k(\sigma)|^2], \quad (3.48)$$

$$\langle \hat{p}_{\text{gw}} \rangle = \frac{1}{a^6} \int \frac{d^3 k}{(2\pi)^3} \left[|G_k(\sigma)|^2 - \frac{\Omega^2}{3} |F_k(\sigma)|^2 \right]. \quad (3.49)$$

Equations (3.48) and (3.49) imply $\partial_\sigma \langle \hat{\rho}_{\text{gw}} \rangle + 3\mathcal{F} \langle \hat{\rho}_{\text{gw}} + \hat{p}_{\text{gw}} \rangle = 0$ provided the evolution equations of F_k and G_k are the ones given in Eq. (3.8).

In order to keep track of the possible ambiguities related with the definitions of the energy-momentum pseudo-tensor we will first perform the calculations within the approach defined by Eqs. (3.43), (3.44) and (3.45). Then, for each dynamical quantity, the results will be compared with the answers obtained using the approach defined by Eqs. (3.48) and (3.49).

4 Effective barotropic indices

As a consequence of the dynamical evolution of the background the energy and pressure densities have a steep (violet) spectrum. Using the results of the previous section, it appears, for instance that for $k < k_{\text{max}}$ we will have, qualitatively, that the logarithmic spectrum of the energy density is ⁹

$$a^4 \frac{d\rho_{\text{gw}}}{d \ln k} \simeq k^4 |c_-(k)|^2, \quad (4.1)$$

where the initial zero-point energy has been already subtracted. For $k > k_{\text{max}}$ the mixing coefficient is not enhanced logarithmically, but rather exponentially suppressed (see Fig. 4 where this aspect is numerically illustrated). Consequently it is plausible that the integrals appearing in the averaged energies and pressure densities are dominated by the modes that are maximally amplified, i.e. $\kappa \simeq \kappa_{\text{max}}$. Since $\kappa_{\text{max}} \simeq 1$, $k_{\text{max}} = 1/\sigma_b$ (see Fig. 4). The direct calculation supports this view since integrals of the energy density can be performed numerically. Let us then define, for practical reasons,

$$a^6 \rho_{\text{gw}} = \int^{k_{\text{max}}} \mathcal{A}_{1,2}(k, \sigma) d \ln k, \quad (4.2)$$

where the indices 1 and 2 refer to the two different parametrizations of the energy density of the relic gravitons discussed respectively, in Eqs. (3.43) and (3.48). In Fig. 5 (left plot) the numerical evaluation of ρ_{gw} is reported. The initial conditions for the mode functions are the ones specified in the previous section for each k -mode. With the dashed line the energy density discussed in Eq. (3.48) is illustrated. With the full line the energy density of Eq. (3.43) is instead reported. The integral appearing in Eq. (4.2) is indeed dominated by the upper limit. This aspect is also illustrated, in a related perspective from the right plot of Fig. 5 where the contribution of the integrand for $\kappa \ll 1$ is reported for a sample of k -modes. In practice, it is useful to specify a given κ_{min} , i.e. the lower limit of integration appearing in Eq. (4.2). For instance, typical values chosen

⁹In the following sections, for sake of simplicity, the averages $\langle \hat{\rho}_{\text{gw}} \rangle$ will be denoted simply by ρ_{gw} and similarly for the the pressure densities.

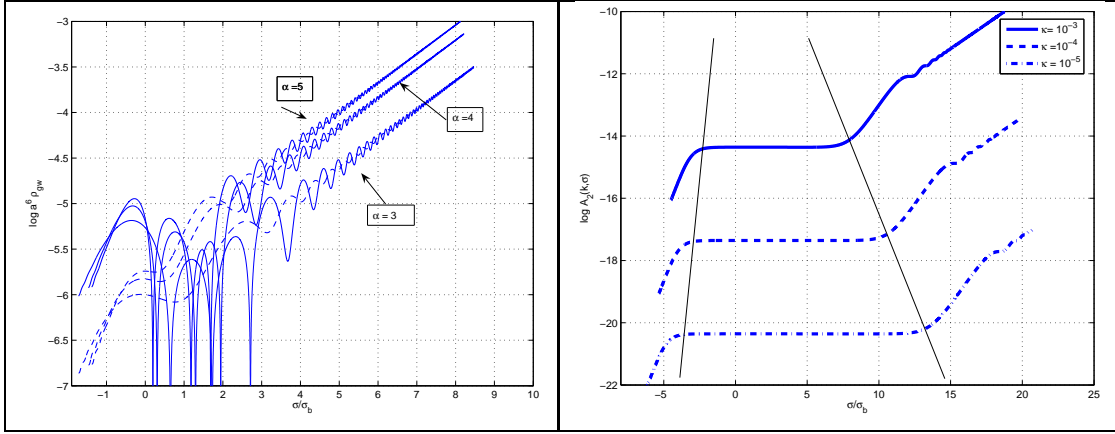


Figure 5: Numerical evaluation (left plot) of the integrated energy density for different values of α . The contribution of a sample of k -modes for the case $\alpha = 4$. Initial conditions for the background are fixed in such a way that $\sigma_1 = \sigma_2 = 0$, while the gauge coupling at the bounce is of order 1. The initial conditions for the tensor modes are the ones dictated by quantum mechanics (see Section 3).

for the present examples are $\kappa = 10^{-12}$ or $\kappa = 10^{-10}$. Since the spectrum is dominated by κ_{\max} , different choices κ_{\min} produce the same results for the integrated energy density. According to Eq. (3.13), κ_{\min} determines a minimal σ_{ex} , i.e. $\sigma_{\text{ex}}(\kappa_{\min})$. This implies that, to be consistent, the initial conditions for the field operators have been given for $\sigma_i \ll \sigma_{\text{ex}}(\kappa_{\min})$ so that, at the initial time, all the tensor modes were of short wavelength.

The right panel of Fig. 5 has some interesting features that will now be discussed. Within the region limited by the two diagonal lines the corresponding modes satisfy $|\kappa\tau| < 1$. Bearing in mind Eq. (4.2), we then have that for modes of long wavelength $a^6\rho_{\text{gw}}$ is constant. Outside the region marked by the two diagonal lines the corresponding modes satisfy $|\kappa\tau| > 1$. In this region $a^6\rho_{\text{gw}}$ increases as a^2 , i.e. $\rho_{\text{gw}} \sim a^{-4}$.

These considerations suggest that in the short wavelength limit the effective barotropic index is the one of radiation, i.e. $1/3$. In fact, in the short wavelength limit the approximate evolution of the mode functions is simply given by Eqs. (3.9) and (3.9). Inserting these solutions either in Eqs. (3.43)–(3.45) or in Eqs. (3.48)–(3.49) the results are the same for both parametrizations. In the long wavelength limit, according to Fig. 5 we should instead have that the effective barotropic index is close to 1.

To corroborate the numerical result, we can solve, directly in the conformal time parametrization, the evolution equations of the mode functions in the approximate background of Eqs. (2.33) and (2.35). The (averaged) energies and pressure densities will then be computed and the result

expanded in the limit of $k\tau \ll 1$.

Following this procedure (see appendix B and, in particular Eqs. (B.29) and (B.30)), from Eqs. (3.48) and (3.49), we have for $\tau < -\tau_1$:

$$\begin{aligned}\rho_{\text{gw}} &\simeq \frac{1}{a^4} \int \frac{k^4}{2\pi^2} d\ln k \left[\frac{1}{(-\pi k\tau)} + \mathcal{O}(k\tau) \right], & \tau < -\tau_1 \\ p_{\text{gw}} &\simeq \frac{1}{a^4} \int \frac{k^4}{2\pi^2} d\ln k \left[\frac{1}{(-\pi k\tau)} + \mathcal{O}(k\tau) \right], & \tau < -\tau_1.\end{aligned}\quad (4.3)$$

Thus, from Eqs. (4.3) we have that, for $k\tau \ll 1$, $p_{\text{gw}} = \rho_{\text{gw}}$. Furthermore, recalling that, for $\tau < -\tau_1$, $a(\tau) \sim \sqrt{-\tau}$, we have as expected that ρ_{gw} and p_{gw} scale as a^{-6} .

If the energy-momentum pseudo-tensor is derived from the quadratic corrections to the Einstein tensor, the ratio between the pressure and the energy densities becomes, for $k\tau \ll 1$,

$$\frac{\mathcal{P}_{\text{gw}}}{\rho_{\text{gw}}} = 1 - \frac{5}{3} \frac{1}{[1 - 4\gamma + 4\ln 2 - 4\ln(-k\tau)]}, \quad (4.4)$$

where γ is the Euler-Mascheroni constant. Notice that this result is consistent with the one of Eqs. (4.3) with the difference that in Eq. (4.4) logarithmic corrections do appear.

It is instructive to compare the present case with the one of a sudden transition from a de Sitter stage of expansion to a radiation-dominated stage of expansion. The typical time-scale τ_1 will now mark the transition from a de Sitter stage of expansion to a radiation-dominated epoch and the analytical form of the scale factor in the two regions is:

$$a(\tau) = -\frac{\tau_1}{\tau}, \quad \tau \leq -\tau_1, \quad (4.5)$$

$$a(\tau) = \frac{\tau + 2\tau_1}{\tau_1}, \quad \tau > -\tau_1. \quad (4.6)$$

In this case (see appendix B for further details), Eqs. (3.43)-(3.45) imply, for $\tau < -\tau_1$,

$$\rho_{\text{gw}} = \frac{1}{a^4} \int \frac{k^4}{2\pi^2} d\ln k \left[1 - \frac{7}{2x^2} \right], \quad (4.7)$$

$$\mathcal{P}_{\text{gw}} = p_{\text{gw}} = \frac{1}{3a^4} \int \frac{k^4}{2\pi^2} d\ln k \left[1 + \frac{7}{2x^2} \right], \quad (4.8)$$

where $x = k\tau$. The energy-density is positive for $k\tau \gg 1$ but it becomes negative when the relevant modes become larger than the Hubble radius, i.e. for $k\tau \ll 1$. The equation of state has an effective barotropic index $1/3$, for $k\tau \gg 1$. In the opposite limit, i.e. $k\tau \ll 1$ the effective barotropic index becomes $-1/3$. From Eqs. (4.7) and (4.8) the energy and pressure densities scale as a^{-2} and this is consistent with Eq. (3.38) for the equation of state $\mathcal{P}_{\text{gw}} = -\rho_{\text{gw}}/3$.

Consider then the case of modes $k\tau \ll 1$ for $\tau > -\tau_1$ i.e. during the radiation-dominated epoch. The exact results are reported in the appendix and here only the long wavelength limit

will be given. As as the approach defined by Eqs. (3.33)–(3.34) is concerned, the relevant results are reported in Eqs. (B.13), (B.15) and (B.16) of the appendix. To lowest order in $|k\tau| \ll 1$ and $|k\tau_1| \ll 1$ Eq. (B.13) leads to

$$\rho_{\text{gw}} = -\frac{5}{6} \frac{1}{a^2} \int \frac{d \ln k}{2\pi^2 \tau_1^4} k^2. \quad (4.9)$$

In the same limit, from Eqs. (B.15) the following result

$$p_{\text{gw}} = \frac{7}{6} \frac{1}{a^2} \int \frac{d \ln k}{2\pi^2 \tau_1^4} k^2, \quad (4.10)$$

can be obtained. We can immediately notice that $p_{\text{gw}}/\rho_{\text{gw}} = -\frac{7}{5}$, which agrees with the calculation of [36, 37]. The fact that the averaged energy density can have negative values for a limited amount of time was noticed, in a related context, in [59].

Finally, from Eq. (B.16), to lowest order in $|x| \ll 1$ and $|x_1| \ll 1$,

$$\mathcal{P}_{\text{gw}} - p_{\text{gw}} = -\frac{8}{9} \frac{1}{a^2} \int \frac{d \ln k}{2\pi^2 \tau_1^4} k^2. \quad (4.11)$$

Therefore, putting together the results expressed in Eqs. (4.9), (4.10) and (4.11), the following chain of equalities holds

$$p_{\text{gw}} = -\frac{7}{5} \rho_{\text{gw}}, \quad (4.12)$$

$$\mathcal{P}_{\text{gw}} = -\frac{7}{5} \rho_{\text{gw}} + \frac{16}{15} \rho_{\text{gw}} = -\frac{1}{3} \rho_{\text{gw}}. \quad (4.13)$$

These results coincide with the ones obtained in [36, 37].

Instead of using the energy-momentum pseudo-tensor derived from the quadratic corrections to the Einstein tensor, we could use the energy and pressure densities discussed in Eqs. (3.46) and (3.47). The relevant results, in this case, are reported in Eqs. (B.18) and (B.19) of the appendix. Again, to lowest order in $|x| \ll 1$ and $|x_1| \ll 1$, Eqs. (B.18) and (B.19) lead to

$$\rho_{\text{gw}} = \frac{1}{2a^4} \int \frac{k^4}{2\pi^2} d \ln k \frac{x^2}{x_1^4} \left[1 - \frac{2}{9} x^2 + \dots \right], \quad (4.14)$$

$$p_{\text{gw}} = -\frac{1}{6a^4} \int \frac{k^4}{2\pi^2} d \ln k \frac{x^2}{x_1^4} \left[1 - \frac{6}{9} x^2 + \dots \right], \quad (4.15)$$

where the ellipses stand for higher-order corrections. While in the case of Eq. (4.9) the averaged energy density is negative, in the case of Eq. (4.14) the averaged energy density is positive. Moreover, from Eqs. (4.14) and (4.15) we have that the effective equation of state in the long wavelength limit is given by

$$p_{\text{gw}} = -\frac{1}{3} \rho_{\text{gw}}, \quad (4.16)$$

which is the same of Eq. (4.13).

Therefore, we can conclude that both in the bouncing case and in the transition from de Sitter to radiation the two parametrizations of the energy-momentum pseudo-tensor give the same information. In particular, \mathcal{P}_{gw} defined by means of the corrections to the Einstein tensor obeys the same equation of state obeyed, in the approach of Eqs. (3.46) and (3.47) by p_{gw} .

5 Iterative calculations of back-reaction effects

The evolution equations including the dynamical effects of the produced gravitons reduce to an integro-differential system whose numerical solution may be obtained by means of iterative methods that we are now going to describe and exploit. One of the important qualitative features of the bounce solutions discussed in Section 2 was expressed by the Eq. (2.13) whose form becomes now

$$\frac{d}{d\sigma} \left(\mathcal{F} + \frac{\xi}{2} \right) = \frac{a^6}{4} (\rho_{\text{gw}} - p_{\text{gw}}), \quad (5.1)$$

where with ρ_{gw} and p_{gw} we denote the averages of the components of the energy-momentum pseudo-tensor of the relic gravitons. To this equation the evolution equation for ξ should be added, i.e.

$$\frac{d\xi}{d\sigma} = -e^\phi a^6 \left[V - \frac{\partial V}{\partial \phi} \right], \quad (5.2)$$

which is (formally) independent on the energy and pressure densities of the created gravitons. The dynamical quantities appearing in Eq. (5.1) and (5.2) are subjected to the following (generalized) Hamiltonian constraint:

$$\mathcal{F}^2 = \frac{a^6}{6} \rho_{\text{gw}} + \frac{\xi^2}{12} + \frac{e^\phi a^6}{6} V, \quad (5.3)$$

that has to be satisfied along the different steps of the numerical solution. Recalling the examples given in Fig. 5, ρ_{gw} and p_{gw} are computed by integrating the evolution equations of the mode functions, i.e. Eqs. (3.8). In this sense, Eq. (5.1) is actually an integro-differential equation whose explicit form is indeed

$$\frac{d}{d\sigma} \left[\mathcal{F} + \frac{\xi}{2} \right] = \frac{1}{4} \int^{k_{\text{max}}} \mathcal{B}(\Omega, \sigma) d \ln k, \quad (5.4)$$

where the quantity $\mathcal{B}(\Omega, \sigma)$ depends on the specific form of the energy-momentum pseudo-tensor. In particular, subtracting Eq. (3.49) from Eq. (3.48)

$$\mathcal{B}(\Omega, \sigma) = \frac{2k^3}{3\pi^2} [\Omega^2(\sigma) |F_k(\sigma)|^2 - \Omega(\sigma)]. \quad (5.5)$$

Similarly, taking the difference between Eq. (3.43) and (3.44)

$$\mathcal{B}(\Omega, \sigma) = \frac{2k^3}{3\pi^2} \{ 2|G_k(\sigma)|^2 - \Omega^2(\sigma) |F_k(\sigma)|^2 + 3\mathcal{F} [F_k(\sigma)^* G_k(\sigma) + F_k(\sigma) G_k(\sigma)^* - \Omega(\sigma)] \}. \quad (5.6)$$

In both equations $F_k(\sigma)$ and $G_k(\sigma)$ satisfy Eqs. (3.8). Note that in Eqs. (5.5) and (5.6) the zero-point energy and pressure densities have been subtracted as discussed in Section 4.

Equation (5.4) can be solved by iteration¹⁰. In fact, from Eq. (5.4) the following hierarchy of equations can be deduced:

$$\mathcal{F}_0(\sigma) + \frac{\xi_0(\sigma)}{2} = 0, \quad (5.7)$$

$$\mathcal{F}_1(\sigma) + \frac{\xi_1(\sigma)}{2} = \frac{1}{4} \int^\sigma d\sigma' \int_0^{k_{\max}} \mathcal{B}_0(\Omega(\sigma'), \sigma') d \ln k, \quad (5.8)$$

$$\mathcal{F}_2(\sigma) + \frac{\xi_2(\sigma)}{2} = \frac{1}{4} \int^\sigma d\sigma' \int_0^{k_{\max}} \mathcal{B}_1(\Omega(\sigma'), \sigma') d \ln k, \quad (5.9)$$

and so on.

The subscripts appearing in the various dynamical quantities of Eqs. (5.7), (5.8) and (5.9) denote the order of the iteration. The source term appearing in the hierarchy is computed from the previous order. So, to zeroth order, i.e. Eq. (5.7), \mathcal{F}_0 and ξ_0 are simply the solutions discussed in Section 2. These solutions will be used to obtain numerically the mode functions that will determine $\mathcal{B}_0(\Omega, \sigma)$. To first order, \mathcal{F}_1 and ξ_1 will be determined from the the zeroth order source, i.e. $\mathcal{B}_0(\Omega, \sigma)$. This will lead to the first-order mode functions allowing the quantitative determination of $\mathcal{B}_1(\Omega, \sigma)$ and so on.

Based on the results of the previous section, the strongest effect is expected from modes of high wave-number (i.e. small wavelength). The rationale for this expectation is that in the long wavelength limit $a^6(\rho_{\text{gw}} - p_{\text{gw}})$, is smaller than the energy density of the dilaton and also approximately vanishing. In the short wavelength limit $a^6(\rho_{\text{gw}} - p_{\text{gw}})$ increases as a^2 and it is expected to dominate the background at sufficiently late times: as time goes by more and more modes will contribute to the ultraviolet branch of the energy spectrum. For the numerical solution of the problem the (stiff) Rosenbrok method [61] has been used. In Fig. 6 the back-reaction effects are reported for the case of a zeroth-order solution with $\alpha = 4$. With the dashed line the zeroth-order iterative solution is illustrated. With the full line the combined effect of the first-order iteration is illustrated. In a radiation-dominated Universe the evolution equation obeyed by $\mathcal{F}(\sigma)$ is simply given by

$$\frac{d\mathcal{F}}{d\sigma} = \mathcal{F}^2, \quad \mathcal{F}^2 = \frac{a^6}{4} \rho_{\text{r}}, \quad (5.10)$$

where ρ_{r} is a generic radiation fluid with $p_{\text{r}} = \rho_{\text{r}}/3$. As already noticed in connection with Eq. (2.41) the first of the two relations appearing in Eq. (5.10) implies that the Ricci scalar vanishes in a radiation-dominated Universe. The behaviour of the solution for $\sigma \gg \sigma_{\text{b}}$, illustrated by the full lines in Fig. 6, corresponds, indeed to the one of a radiation-dominated Universe in the σ

¹⁰It should be mentioned that an iterative approach for the solution of the back-reaction problems has been also invoked by the authors of Ref. [60].

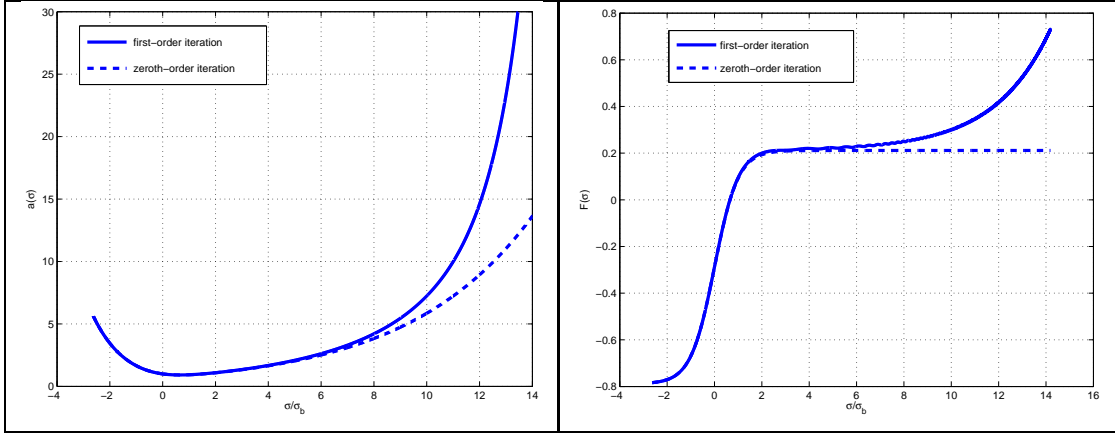


Figure 6: The evolution of the scale factor (left plot) and of \mathcal{F} (right plot) in the case $\alpha = 4$. The back-reaction effects are implemented using the Eq.(5.5). The parameters of the zeroth order solution are fixed by requiring $\sigma_1 = \sigma_2 = 0$ and $\phi_b = 0$.

parametrization. In this parametrization, in fact $\mathcal{F} \simeq (\sigma - \sigma_*)^{-1}$ and \mathcal{F}/a is constant. This non-standard evolution of the scale factor becomes more familiar by translating the result from the σ -parametrization to the τ parametrization. Recalling, in fact, that $a(\sigma)^2 d\sigma = d\tau$, we do find that $\tau \simeq (\sigma - \sigma_*)^{-1}$. This occurrence implies, as expected, that $a(\tau) \simeq \tau$ which is the well known result for a radiation-dominated Universe in the conformal time parametrization.

In Fig. 6 the back-reaction effects have been implemented by using Eq. (5.5) which comes from Eqs. (3.48) and (3.49). In Fig. 7 the numerical calculation has been instead performed by using Eq. (5.6). By comparing Fig. 6 with Fig. 7 the main visible effect is an enhanced oscillating behaviour of the first-order iteration after the bounce. However, the evolution of the scale factor and of \mathcal{F} is clearly the same.

The iterative method described in the present Section can be also applied in the conformal time parametrization. We will omit here the technical details but the general idea is to start with the asymptotic solution valid for $\tau \ll -\tau_1$ (which is, for instance the one provided by Eqs. (2.33) and (2.35)) and then integrate numerically both for the background and for the fluctuations. The main technical difference between the integration in the σ and in the τ parametrization is the following. In the σ parametrization the analytical solution of Eqs. (2.26) and (2.27) can be used in the zeroth-order iteration. In the τ parametrization already the zeroth order iteration requires numerical treatment. Moreover, in the τ parametrization the evolution equations for the mode functions are formally different and are the ones reported in Eq. (B.22) of the Appendix B.

In Fig. 8 the integration of the iterative problem is illustrated in the τ parametrization. With

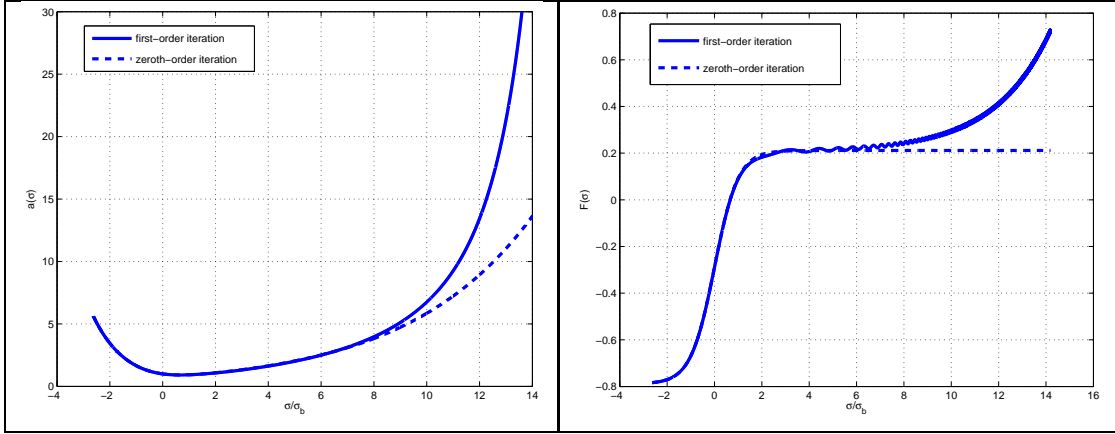


Figure 7: The same quantities reported in Fig. 6 but using implementing the back-reaction effects through the energy and pressure densities stemming from the quadratic corrections to the Einstein tensor (i.e. Eq. (5.6)).

the dashed line the zeroth-order solution is reported. With the full line the result of the first iteration is illustrated. In the left plot of Fig. 8 the parameters are chosen to be the same ones of Figs. 6 and 7. In the right plot the value of the gauge coupling at the bounce is chosen to be much smaller than 1. This implies that the scale factor after the bounce is much larger than in the case when the gauge coupling is of order 1 at the bounce. This can be understood analytically since the asymptotic zeroth-order solution (i.e. Eq. (2.34) leads to a scale factor whose absolute normalization increases as the gauge coupling at the bounce diminishes. It is evident from Fig. 8 that the first-order iteration already leads to a scale factor that increases linearly in conformal time. For both plots in Fig. 8 the back-reaction effects has been parametrized through the analog of Eq. (5.5), appropriately translated in the τ parametrization.

6 Concluding remarks

Dynamical back-reaction of relic gravitons is relevant in different contexts, so that the nature of the induced physical effects may vary. A particularly interesting situation is the one of bouncing solutions of pre-big bang type where back-reaction effects are known to be important already from qualitative estimates. One of the purposes of the present investigation is to propose a theoretical scheme where more quantitative predictions could be derived. The present findings are then useful for implementing a smooth exit from the pre-big bang phase with consequent production of radiation. The bouncing solutions examined here may also be viewed as a practical theoretical laboratory where the methods for the analysis of the back-reaction effects of relic gravitons may

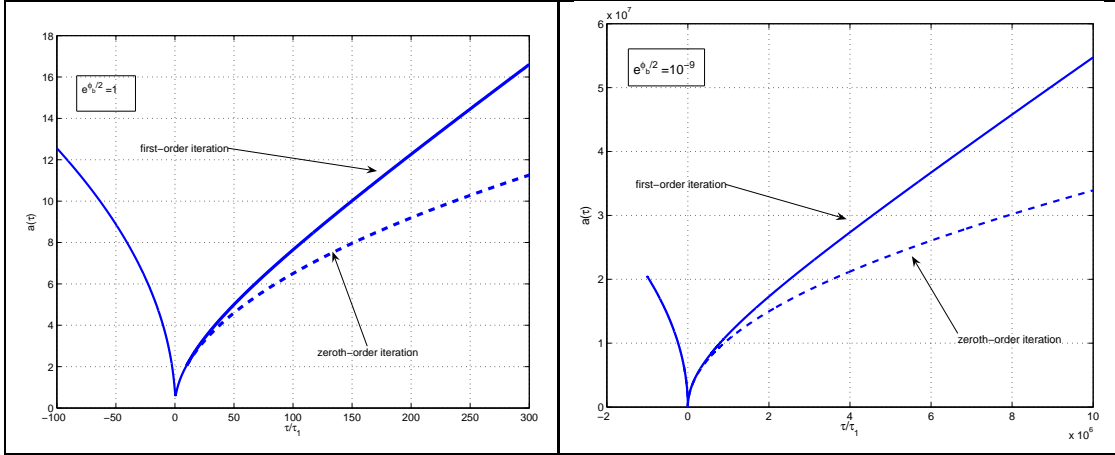


Figure 8: Integration of the iterative problem in the conformal time parametrization. In the left plot the parameters of the zeroth-order solution coincide (in the limit $\tau \rightarrow -\infty$) with the parameters chosen for the integrations reported in Figs. 6 and 7 (for $\sigma \rightarrow -\infty$).

be tested. In this respect, the reported results suggest that the rôle of the produced gravitons is crucial for determining the asymptotic state of the solution at late times.

The strategy followed in the present analysis relies on the interplay between analytical methods and numerical calculations. We have been interested in situations where the Universe undergoes an accelerated contraction before the bounce, while, after the bounce, the zeroth-order solution exhibits a decelerated expansion. After quantizing the tensor modes of the geometry, the initial values of the field operators have been set well before the bounce. At that time all the gravitons were of short-wavelengths in comparison with the typical time scale of the background evolution. Then, the field operators have been evolved in the Heisenberg representation and the mixing coefficients have been accurately determined both analytically and numerically. This step allowed to understand what kind of regularization is required for the energy and pressure densities of the produced gravitons. The second step has been to adopt a consistent ansatz for the gravitational energy-momentum pseudo-tensor. Two complementary definitions of the energy and pressure densities of the relic gravitons have then been scrutinized and compared both analytically and numerically. On the basis of the reported results, these two different approaches lead to compatible quantitative results.

The self-consistent analysis of back-reaction effects leads naturally to an integro-differential problem. Consequently, an iterative method for its solution has been proposed and tested in the specific dynamical framework of bouncing solutions that arise in the context of the low-energy string effective action supplemented by a non-local dilaton potential. It turns out that the treatment both of the background and of the tensor fluctuations becomes rather simple by selecting a different

parametrization of the time coordinate which does not coincide with the usual conformal or cosmic times. In this time parametrization analytical bouncing solutions can be derived in the Einstein frame metric.

By looking at the structure of the low-energy string effective action, it is possible to infer that not only relic gravitons but also other massless fields may lead to similar effects whose analysis is certainly one of the possible developments of future studies. In this respect, the present investigation dealt with the minimal field content of the model with the aim of achieving a reasonably accurate description of the underlying physical processes. Thus, some of the ideas discussed here will hopefully be useful also for the description of dynamical systems with a richer field content.

A Energy-momentum pseudo-tensor

From Eq. (1.1) we have

$$\delta_t^{(1)} g_{ij} = -a^2 h_{ij}, \quad h_i^i = \partial_i h_j^i = 0, \quad (\text{A.1})$$

where, as in the bulk of the paper, the subscript refers to the tensor nature of the fluctuation while the superscript denotes the perturbative order. Equation (A.1) implies that

$$\delta_t^{(1)} g^{ij} = \frac{h^{ij}}{a^2}, \quad \delta_t^{(2)} g^{ij} = -\frac{h_k^i h^{kj}}{a^2}. \quad (\text{A.2})$$

Consequently, the fluctuations of the Christoffel connections to first and second order become:

$$\begin{aligned} \delta_t^{(1)} \Gamma_{ij}^0 &= \frac{1}{2}(h'_{ij} + 2\mathcal{H}h_{ij}), \\ \delta_t^{(1)} \Gamma_{i0}^j &= \frac{1}{2}h_i^{j'}, \\ \delta_t^{(1)} \Gamma_{ij}^k &= \frac{1}{2}(\partial_i h_j^k + \partial_j h_i^k - \partial^k h_{ij}), \\ \delta_t^{(2)} \Gamma_{i0}^j &= -\frac{1}{2}h^{ik} h'_{kj}, \\ \delta_t^{(2)} \Gamma_{ij}^k &= \frac{1}{2}h^{i\ell} [\partial_\ell h_{jk} - \partial_k h_{j\ell} - \partial_j h_{k\ell}], \end{aligned} \quad (\text{A.3})$$

where, as in the bulk of the paper, the prime denotes a derivation with respect to the conformal time coordinate. The fluctuations of the various components of the Ricci tensor to first and second order are then:

$$\delta_t^{(1)} R_{ij} = \frac{1}{2}[h''_{ij} + 2\mathcal{H}h'_{ij} - \nabla^2 h_{ij}] + (\mathcal{H}' + 2\mathcal{H}^2)h_{ij}, \quad (\text{A.4})$$

$$\delta_t^{(2)} R_{00} = \frac{1}{4}h'_{ij} h^{ij'} - \frac{\mathcal{H}}{2}h_{ij} h^{ij'} + \frac{1}{2}h^{ij} \nabla^2 h_{ij}, \quad (\text{A.5})$$

$$\begin{aligned} \delta_t^{(2)} R_{ij} &= \frac{1}{2}h^{k\ell} [\partial_k \partial_\ell h_{ij} - \partial_k \partial_j h_{\ell i} - \partial_k \partial_i h_{j\ell}] \\ &\quad - \frac{1}{2} \partial_j [h^{k\ell} (\partial_\ell h_{ik} - \partial_k h_{\ell i} - \partial_i h_{k\ell})] - \frac{\mathcal{H}}{2} h^{k\ell} h'_{k\ell} \delta_{ij} \\ &\quad + \frac{\mathcal{H}}{2} h_j^\ell h'_{\ell i} + \frac{\mathcal{H}}{2} h_i^\ell h'_{\ell j} - \frac{1}{4} h_j^{k'} h'_{ik} - \frac{\mathcal{H}}{2} h_j^{k'} h_{ik} - \frac{1}{4} h_i^{k'} h'_{kj} - \frac{\mathcal{H}}{2} h_i^{k'} h_{kj} \\ &\quad - \frac{1}{4} [\partial_i h_k^\ell + \partial_k h_i^\ell - \partial^\ell h_{ik}] [\partial_\ell h_j^k + \partial_j h_\ell^k - \partial^k h_{j\ell}]. \end{aligned} \quad (\text{A.6})$$

The Ricci scalar is zero to first order in the tensor fluctuations, i.e. $\delta_t^{(1)} R = 0$. This is due to the traceless nature of these fluctuations. To second-order, however, $\delta_t^{(2)} R \neq 0$ and its form is:

$$\begin{aligned} \delta_t^{(2)} R &= \frac{1}{a^2} \left\{ \frac{3}{4} h'_{k\ell} h^{k\ell'} + \mathcal{H} h'_{k\ell} h^{k\ell} + \frac{1}{2} h^{k\ell} \nabla^2 h_{k\ell} - \frac{1}{4} \partial_i h^{k\ell} \partial^i h_{k\ell} \right\} \\ &\quad + \frac{1}{a^2} \left\{ -\frac{1}{2} \partial_i [h^{k\ell} (\partial_\ell h_k^i - \partial_k h_\ell^i - \partial^i h_{k\ell})] \right. \\ &\quad \left. - \frac{1}{4} [\partial_i h_k^\ell \partial_\ell h_i^k - \partial_i h_k^\ell \partial^k h_{i\ell} + \partial_k h^{\ell i} \partial_\ell h_i^k - \partial^\ell h_{ik} \partial^i h_\ell^k + \partial^\ell h_{ik} \partial^k h_{i\ell}] \right\}. \end{aligned} \quad (\text{A.7})$$

Recalling the form of the Einstein tensor (see Eq. (1.2)),

$$\delta_t^{(2)} \mathcal{G}_{00} = -\ell_{\text{P}}^2 \mathcal{T}_{00} = \delta_t^{(2)} R_{00} - \frac{1}{2} \bar{g}_{00} \delta_t^{(2)} R, \quad (\text{A.8})$$

we obtain

$$\ell_{\text{P}}^2 \mathcal{T}_{00} = \mathcal{H} h'_{k\ell} h^{k\ell} + \frac{1}{8} (h'_{k\ell} h^{k\ell'} + \partial_i h_{k\ell} \partial^i h^{k\ell}) + \mathcal{D}_{00}, \quad (\text{A.9})$$

where \mathcal{D}_{00} is a total derivative, i.e.

$$\mathcal{D}_{00} = \frac{1}{8} \partial_\ell [\partial_i h^{k\ell} h_k^i - 2 \partial_k h_i^\ell h^{ki}] \quad (\text{A.10})$$

From Eqs. (A.6) and (A.7) it is also possible to write:

$$\begin{aligned} \delta_t^{(2)} R_{ij} &= \frac{1}{4} (\partial_k h_i^\ell \partial^k h_{j\ell} + \partial^\ell h_{ik} \partial_\ell h_j^k) - \frac{1}{4} \partial_i h_{k\ell} \partial_j h^{k\ell} \\ &\quad - \frac{\mathcal{H}}{2} h^{k\ell} h'_{k\ell} \delta_{ij} + \frac{\mathcal{H}}{2} (h_j^\ell h_{\ell i} + h_i^\ell h_{\ell j}) \\ &\quad - \frac{\mathcal{H}}{2} (h_j^{k'} h_{ik} + h_i^{k'} h_{kj}) - \frac{1}{4} (h_j^{k'} h'_{ik} + h_i^{k'} h'_{kj}) + \mathcal{D}_{ij}, \\ \delta_t^{(2)} R &= \frac{1}{a^2} \left[\frac{3}{4} h'_{k\ell} h^{k\ell'} + \mathcal{H} h'_{k\ell} h^{k\ell} - \frac{3}{4} \partial_i h^{k\ell} \partial^i h_{k\ell} \right] + \frac{1}{a^2} \mathcal{D}_R, \end{aligned} \quad (\text{A.11})$$

where \mathcal{D}_{ij} and \mathcal{D}_R are further total derivative

$$\begin{aligned} \mathcal{D}_{ij} &= \frac{1}{2} \partial_k [h^{k\ell} (\partial_\ell h_{ij} - \partial_j h_{i\ell} - \partial_i h_{j\ell})] - \frac{1}{2} \partial_j [h^{k\ell} (\partial_\ell h_{ik} - \partial_k h_{\ell i} - \partial_i h_{k\ell})] \\ &\quad - \frac{1}{4} \partial_\ell [\partial_k h_i^\ell h_j^k + h_{ik} \partial^k h_j^\ell], \\ \mathcal{D}_R &= \partial_i [h^{k\ell} \partial^i h_{k\ell}] + \frac{1}{4} \partial_\ell [\partial_i h^{k\ell} h_k^i - 2 \partial_k h_i^\ell h^{ki}], \end{aligned} \quad (\text{A.12})$$

Therefore, up to total derivatives, the following result holds:

$$\ell_{\text{P}}^2 \mathcal{T}_{00} = \mathcal{H} h'_{k\ell} h^{k\ell} + \frac{1}{8} (h'_{k\ell} h^{k\ell'} + \partial_i h_{k\ell} \partial^i h^{k\ell}), \quad (\text{A.13})$$

and

$$\ell_{\text{P}}^2 \mathcal{T}_{ij} = \frac{3}{8} \delta_{ij} [\partial_m h_{k\ell} \partial^m h^{k\ell} - h'_{k\ell} h^{k\ell'}] + \frac{1}{2} h_j^{k'} h'_{ik} + \frac{1}{4} \partial_i h_{k\ell} \partial_j h^{k\ell} - \frac{1}{2} \partial_k h_i^\ell \partial^k h_{\ell j}. \quad (\text{A.14})$$

To pass from doubly covariant indices to mixed ones, it is useful to recall that, to second order,

$$\delta^{(2)} \mathcal{G}_\mu^\nu = \delta^{(2)} [g^{\nu\alpha} \mathcal{G}_{\mu\alpha}] = \delta^{(2)} g^{\nu\alpha} \bar{\mathcal{G}}_{\mu\alpha} + \bar{g}^{\nu\alpha} \delta^{(2)} \mathcal{G}_{\mu\alpha} + \delta^{(1)} g^{\nu\alpha} \delta^{(1)} \mathcal{G}_{\mu\alpha}. \quad (\text{A.15})$$

By looking at the form of the specific terms arising in the previous equation it is clear that $\mathcal{T}_0^0 = \bar{g}^{00} \mathcal{T}_{00}$ and that $\mathcal{T}_i^j = \bar{g}^{jk} \mathcal{T}_{ki}$. The expressions for \mathcal{T}_0^0 and \mathcal{T}_i^j are the ones reported in Eqs. (3.31) and (3.32) (see also Eqs. (3.33) and (3.34)). These expressions coincide with the ones obtained, for instance, in [36, 37] and are also consistent with the ones of [34, 35].

B Analytical estimates of the effective barotropic indices

Since the Hamiltonian defined in Eq. (3.4) is time-dependent, it is always possible to perform time-dependent canonical transformations, leading to a different form of the Hamiltonian that will be classically equivalent to (3.4). This procedure correspond to drop total time derivatives from the corresponding classical action [62].

From the action (3.3), defining the new field $\mu = ah$ and dropping a total time derivative the following Hamiltonian can be obtained in the τ -parametrization

$$\tilde{H}_{\text{gw}}(\tau) = \frac{1}{2} \int d^3x \left[\pi^2 + (\partial_i \mu)^2 - (\mathcal{H}^2 + \mathcal{H}') \mu^2 \right], \quad (\text{B.1})$$

where $\pi = \mu'$. This form of the Hamiltonian is particularly convenient for the studying the time evolution of the field operators in the conformal time parametrization. By appropriate Fourier transforms of the field operators (see Eq. (3.5)), the analog of Eqs. (3.6) and (3.7) are

$$\begin{aligned} \hat{\mu}_{\vec{k}}(\tau) &= \hat{b}_{\vec{k}}(\tau_i) f_k(\tau) + \hat{b}_{-\vec{k}}^\dagger(\tau_i) f_k^*(\tau), \\ \hat{\pi}_{\vec{k}}(\tau) &= \hat{b}_{\vec{k}}(\tau_i) g_k(\tau) + \hat{b}_{-\vec{k}}^\dagger(\tau_i) g_k^*(\tau), \end{aligned} \quad (\text{B.2})$$

where the new mode functions now obey

$$f_k'' + \left[k^2 - \frac{a''}{a} \right] f_k = 0, \quad g_k = f_k'. \quad (\text{B.3})$$

In the limit $\tau_i \rightarrow -\infty$, the operators $\hat{b}_{\vec{k}}(\tau_i)$ and $\hat{b}_{-\vec{k}}^\dagger(\tau_i)$ annihilate the same initial vacuum state as the one annihilated by $\hat{a}_{\vec{k}}(\sigma_i)$ and $\hat{a}_{-\vec{k}}^\dagger(\sigma_i)$ in the limit $\sigma_i \rightarrow -\infty$.

In this framework all the calculations discussed in the σ -parametrization can be reformulated. The expectation values of the energy and pressure density can be computed. For instance from Eqs. (3.31) and (3.32) we have ¹¹

$$\langle \hat{\rho}_{\text{gw}} \rangle = \frac{1}{a^4} \int \frac{d^3k}{(2\pi)^3} \{ (k^2 - 7\mathcal{H}^2) |f_k(\tau)|^2 + |g_k(\tau)|^2 + 3\mathcal{H} [f_k(\tau) g_k^*(\tau) + f_k^*(\tau) g_k(\tau)] \}, \quad (\text{B.4})$$

$$\begin{aligned} \langle \hat{p}_{\text{gw}} \rangle &= \frac{1}{3a^4} \int \frac{d^3k}{(2\pi)^3} \{ |f_k(\tau)|^2 (7k^2 - 5\mathcal{H}^2) - 5|g_k(\tau)|^2 \\ &+ 5\mathcal{H} [f_k^*(\tau) g_k(\tau) + f_k(\tau) g_k^*(\tau)] \}. \end{aligned} \quad (\text{B.5})$$

$$\langle \hat{\mathcal{P}}_{\text{gw}} \rangle = \langle \hat{p}_{\text{gw}} \rangle + \frac{4(\mathcal{H}^2 - \mathcal{H}')}{3\mathcal{H} a^4} \int \frac{d^3k}{(2\pi)^3} [f_k(\tau) g_k^*(\tau) + f_k^*(\tau) g_k(\tau)]. \quad (\text{B.6})$$

In similar terms, the expectation values of the energy and pressure densities can be obtained within the approach of Refs. [39, 40].

¹¹In the bulk of the paper, for practical reasons, we dropped the expectation values for the averaged quantities. In this appendix, to make clear the computational procedures, the expectation values will be restored.

Consider now the case of a transition from a de Sitter stage of expansion to a radiation-dominated stage of expansion, i.e. Eqs. (4.5) and (4.6). For $\tau \leq -\tau_1$,

$$f_k(\tau) = \frac{1}{\sqrt{2k}} \left(1 - \frac{i}{x}\right) e^{-ix}, \quad g_k(\tau) = i\sqrt{\frac{k}{2}} \left[\frac{1}{x^2} - 1 + \frac{i}{x}\right] e^{-ix}, \quad (\text{B.7})$$

where $x = k\tau$. For $\tau > -\tau_1$ the canonical fields can be expressed as

$$\hat{\mu}_{\vec{k}}(\tau) = \hat{b}_{\vec{k}} F_k(\tau) + \hat{b}_{-\vec{k}}^\dagger F_k^*(\tau), \quad \hat{\pi}_{\vec{k}}(\tau) = \hat{b}_{\vec{k}} G_k(\tau) + \hat{b}_{-\vec{k}}^\dagger G_k^*(\tau), \quad (\text{B.8})$$

where the mode functions are now

$$F_k(\tau) = \frac{1}{\sqrt{2k}} e^{-i(x+2x_1)}, \quad G_k(\tau) = -i\sqrt{\frac{k}{2}} e^{-i(x+2x_1)}. \quad (\text{B.9})$$

Since the field operators must be continuous we have

$$\begin{aligned} f_k(-\tau_1) &= c_+(k) F_k(-\tau_1) + c_-(k) F_k^*(-\tau_1), \\ \tilde{g}_k(-\tau_1) &= c_+(k) G_k(-\tau_1) + c_-(k) G_k^*(-\tau_1). \end{aligned} \quad (\text{B.10})$$

so that $c_+(k)$ and $c_-(k)$ can be determined as

$$c_+(k) = \frac{e^{2ix_1}(2x_1^2 - 1 + 2ix_1)}{2x_1^2}, \quad c_-(k) = \frac{1}{2x_1^2}, \quad (\text{B.11})$$

where $x_1 = k\tau_1$. It can be verified immediately that $|c_+(k)|^2 - |c_-(k)|^2 = 1$.

It is now instructive to consider the behaviour of the effective barotropic indices in the two regimes $\tau < -\tau_1$ and $\tau > -\tau_1$. Furthermore, in each regime, we shall be interested in the relative weight of the short and long wavelength modes. This analysis is useful for the comparison with the case of bouncing models. Since during the de Sitter phase, $\mathcal{H}' = \mathcal{H}^2$, Eqs. (B.5) and (B.6) imply that $\langle \hat{p}_{\text{gw}} \rangle = \langle \hat{\mathcal{P}}_{\text{gw}} \rangle$. Furthermore, if we will have that $3\langle \rho_{\text{gw}} \rangle = \langle p_{\text{gw}} \rangle$. During the radiation-dominated phase, i.e. $\tau > -\tau_1$, the short wavelength modes also obey a radiative equation of state and the energy and pressure densities explicitly depend upon the mixing coefficients, i.e.

$$\begin{aligned} \langle \hat{\rho}_{\text{gw}} \rangle &= \frac{1}{a^4} \int \frac{k d^3 k}{(2\pi)^3} [2|c_-(k)|^2 + 1], \\ \langle \hat{\mathcal{P}}_{\text{gw}} \rangle &= \langle p_{\text{gw}} \rangle = \frac{1}{3a^4} \int \frac{k d^3 k}{(2\pi)^3} [2|c_-(k)|^2 + 1], \end{aligned} \quad (\text{B.12})$$

where, for simplicity, the vacuum contribution has not been subtracted. Notice that, now (i.e. in the radiation dominated epoch and for $k\tau \gg 1$), the equality of $\langle \hat{\mathcal{P}}_{\text{gw}} \rangle$ and $\langle \hat{p}_{\text{gw}} \rangle$, is a consequence of the explicit form of the mode functions in this regime, i.e. $F_k G_k^* + F_k^* G_k = 0$.

In the long wavelength limit, i.e. $k\tau \ll 1$ and during the de Sitter phase we obtain, instead, the same expressions reported in Eqs. (4.7) and (4.8). Consider finally the last case, i.e. long wavelength

modes during the radiation dominated epoch. After making use of the explicit expressions of the mixing coefficients we will have, for the averaged energy density,

$$\begin{aligned}
\langle \hat{\rho}_{\text{gw}} \rangle &= \frac{1}{a^4} \int \frac{k d^3 k}{(2\pi)^3} \left\{ \frac{1}{2} \left[2 - \frac{7}{(x+2x_1)^2} \right] \left(1 + \frac{1}{2x_1^4} \right) \right. \\
&\quad - \sin 2(x+x_1) \left[\frac{3(2x_1^2-1)}{2(x+2x_1)x_1^4} + \frac{7}{2(x+2x_1)^2 x_1^3} \right] \\
&\quad \left. + \cos 2(x+x_1) \left[\frac{3}{(x+2x_1)x_1^3} - \frac{7(2x_1^2-1)}{4x_1^4(x+2x_1)^2} \right] \right\}, \tag{B.13}
\end{aligned}$$

Consequently, to lowest order in $|x| \ll 1$ and $|x_1| \ll 1$ the averaged energy density will be

$$\langle \hat{\rho}_{\text{gw}} \rangle = -\frac{5}{6} \frac{1}{a^2} \int \frac{d \ln k}{2\pi^2 \tau_1^4} k^2, \tag{B.14}$$

which is the result reported in Eq. (4.9). Along similar lines the averaged pressure density can be obtained:

$$\begin{aligned}
\langle \hat{p}_{\text{gw}} \rangle &= \frac{1}{3a^4} \int \frac{k^4 d \ln k}{2\pi^2} \left\{ \frac{1}{2} \left[2 - \frac{5}{(x+2x_1)^2} \right] \left(1 + \frac{1}{2x_1^4} \right) \right. \\
&\quad + \frac{1}{4x_1^4} \left(12 - \frac{5}{(x+2x_1)^2} \right) [(2x_1^2-1) \cos 2(x+x_1) + 2x_1 \sin 2(x+x_1)] \\
&\quad \left. - \frac{5}{2(x+2x_1)x_1^4} [(2x_1^2-1) \sin 2(x+x_1) - 2x_1 \cos 2(x+x_1)] \right\}, \tag{B.15}
\end{aligned}$$

$$\begin{aligned}
\langle \hat{\mathcal{P}}_{\text{gw}} \rangle - \langle \hat{p}_{\text{gw}} \rangle &= \frac{8}{3a^4} \int \frac{d^3 k}{(2\pi)^3} \left[-\frac{(2x_1^2-1)}{2x_1^4} \sin 2(x+x_1) + \frac{1}{x_1^3} \cos 2(x+x_1) \right. \\
&\quad - \frac{1}{(x+2x_1)} \left(1 + \frac{1}{2x_1^4} \right) - \frac{(2x_1^2-1)}{2xx_1^4} \cos 2(x+x_1) \\
&\quad \left. - \frac{1}{(x+2x_1)x_1^3} \sin 2(x+x_1) \right] \tag{B.16}
\end{aligned}$$

implying, to lowest order in $|x| \ll 1$ and $|x_1| \ll 1$,

$$\langle \hat{p}_{\text{gw}} \rangle = \frac{7}{6} \frac{1}{a^2} \int \frac{d \ln k}{2\pi^2 \tau_1^4} k^2, \quad \langle \hat{\mathcal{P}}_{\text{gw}} \rangle - \langle \hat{p}_{\text{gw}} \rangle = -\frac{8}{9} \frac{1}{a^2} \int \frac{d \ln k}{2\pi^2 \tau_1^4} k^2, \tag{B.17}$$

which are the results reported in Eqs. (4.10) and (4.11).

Instead of using the energy-momentum pseudo-tensor derived from the quadratic corrections to the Einstein tensor, we could use the energy and pressure densities proposed in [39, 40] (see also [6]). In this second case the expectation values of the energy and pressure density become:

$$\begin{aligned}
\langle \hat{\rho}_{\text{gw}} \rangle &= \frac{1}{a^4} \int \frac{k^4}{2\pi^2} d \ln k \left\{ \frac{1}{2} \left[2 + \frac{1}{(x+2x_1)^2} \right] \left(1 + \frac{1}{2x_1^4} \right) \right. \\
&\quad \left. + \cos 2(x+x_1) \left[\frac{(2x_1^2-1)}{4x_1^4(x+2x_1)^2} - \frac{1}{x_1^3(x+2x_1)} \right] \right\}
\end{aligned}$$

$$+ \sin 2(x + x_1) \left[\frac{(2x_1^2 - 1)}{2x_1^4(x + 2x_1)} + \frac{1}{2x_1^3(x + 2x_1)^2} \right] \Big\}, \quad (\text{B.18})$$

$$\begin{aligned} \langle \hat{p}_{\text{gw}} \rangle &= \frac{1}{a^4} \int \frac{k^4}{2\pi^2} d \ln k \left\{ \frac{1}{2} \left(1 + \frac{1}{2x_1^4} \right) \left[\frac{2}{3} + \frac{1}{(x + 2x_1)^2} \right] \right. \\ &+ \cos 2(x + x_1) \left[\frac{2x_1^2 - 1}{4x_1^4} \left(\frac{1}{(x + 2x_1)^2} - \frac{4}{3} \right) - \frac{1}{x_1^3(x + 2x_1)} \right] \\ &\left. + \sin 2(x + x_1) \left[\frac{1}{2x_1^3} \left(\frac{1}{(x + 2x_1)^2} - \frac{4}{3} \right) + \frac{2x_1^2 - 1}{2x_1^4(x + 2x_1)} \right] \right\} \end{aligned} \quad (\text{B.19})$$

If we now expand the previous expressions for $|x_1| \ll 1$ and for $|x| \ll 1$ we get to the results reported in Eqs. (4.14) and (4.15).

In the following we are going to cross check some of the results obtained in the case of the σ parametrization but working directly in the conformal time coordinate. It should be clear that the specific parametrization is not crucial to obtain a given result. However, it can happen that, for practical reasons, a given parametrization has to be preferred since it leads either to more transparent or to swifter results. The idea will be here to solve the evolution of the mode functions exactly but keeping an approximate form of the background in the post-bounce and in the pre-bounce region. In the conformal time parametrization the action given in Eq. (1.4) reads

$$S_{\text{gw}} = \frac{1}{2} \int d^3x d\tau a^2 [(\partial_\tau h)^2 - a^2(\partial_m h)^2], \quad (\text{B.20})$$

whose associate Hamiltonian is

$$H_{\text{gw}} = \frac{1}{2} \int d^3x [\Pi^2 + a^2(\partial_m h)^2], \quad (\text{B.21})$$

with canonical momentum given as $\Pi = a^2 h'$. Therefore in this case the mode functions obey

$$\tilde{f}_k'' + 2\mathcal{H}\tilde{f}_k' + k^2\tilde{f}_k = 0, \quad \tilde{g}_k = a^2\tilde{f}_k'. \quad (\text{B.22})$$

Consider, for instance, the case given in Eqs. (2.33), (2.34) and (2.35). The form of the mode functions before the bounce (i.e. for $\tau < -\tau_1$) will then be

$$\begin{aligned} \tilde{f}_k(\tau) &= \frac{\sqrt{\tau_1\pi}}{\sqrt{2a_-}} e^{i\pi/4} H_0^{(1)}(-x), \\ \tilde{g}_k(\tau) &= -a^2(\tau)k\sqrt{\tau_1}e^{i\pi/4}\sqrt{\frac{\pi}{2}}H_1^{(1)}(-x), \end{aligned} \quad (\text{B.23})$$

where, as in the previous example, $x = k\tau$; $H_\nu^1(z)$ and $H_\nu^{(2)}(z)$ will denote, in the following, the Hankel functions of index ν and argument z [63, 64]. For $\tau > \tau_1$, recalling Eq. (2.34), the evolution of the mode functions can be written as:

$$\begin{aligned} \tilde{F}_k(\tau) &= \frac{\sqrt{\pi}}{\sqrt{2}} \frac{\sqrt{\tau_1}}{a_+} \left[c_+(k) e^{i\pi/4} H_0^{(1)}(x) + c_-(k) e^{-i\pi/4} H_0^{(2)}(x) \right], \\ \tilde{G}_k(\tau) &= -a^2(\tau) \frac{k\sqrt{\tau_1}}{a_+} \sqrt{\frac{\pi}{2}} \left[c_+(k) e^{i\pi/4} H_1^{(1)}(x) + c_-(k) e^{-i\pi/4} H_1^{(2)}(x) \right]. \end{aligned} \quad (\text{B.24})$$

It is now instructive to pretend that the analytical form of the mode functions is unavailable in the intermediate region, i.e. $-\tau_1 < \tau < \tau_1$. Therefore let us try to excise a thin region around the bounce and compute the mixing coefficients by assuming

$$\tilde{f}_k(-\tau_1) = \tilde{F}_k(\tau_1), \quad \tilde{g}_k(-\tau_1) = \tilde{G}_k(\tau_1). \quad (\text{B.25})$$

This allows to determine

$$\begin{aligned} c_+(k) &= -i \frac{\pi}{4} x_1 [H_1^{(2)}(x_1) H_0^{(1)}(x_1) + H_0^{(2)}(x_1) H_1^{(1)}(x_1)], \\ c_-(k) &= -\frac{\pi}{2} x_1 H_0^{(1)}(x_1) H_1^{(1)}(x_1), \end{aligned} \quad (\text{B.26})$$

Notice that from the previous formulas it is possible to obtain, after some trivial algebra, that $|c_+(k)|^2 - |c_-(k)|^2 = 1$. Recalling now that [63, 64]

$$H_0^{(1)}(x_1) \sim i \frac{2}{\pi} \ln x_1, \quad H_1^{(1)}(x_1) \sim -\frac{2i}{\pi x_1} \quad (\text{B.27})$$

we find that for $x_1 \ll 1$

$$c_-(k) \sim -\frac{2}{\pi} \ln x_1 \quad (\text{B.28})$$

Now this result is (qualitatively) similar to the one obtained, by a totally different approach, in Eqs. (3.16), (3.17) and (3.30). By doing a more careful comparison it is possible to show that the method discussed in Section 3 of the present paper is the most accurate, also from a conceptual point of view. However, the path followed in the present appendix is able to reproduce the gross features of the mixing and, therefore, can be used for semi-quantitative estimates.

It is interesting to notice that, within this approach, the results of the effective barotropic indices (numerically obtained in the text) can be checked. For instance, in the approach of [39, 40] the energy and pressure densities before the bounce become, in the present example

$$\begin{aligned} \langle \hat{\rho}_{\text{gw}} \rangle &= \frac{1}{a^4} \int \frac{k^4}{2\pi^2} d \ln k \left\{ \frac{\pi}{4} (-x) [J_1(-x)^2 + Y_1(-x)^2 + J_0(-x)^2 + Y_0(-x)^2] \right\}, \\ \langle \hat{p}_{\text{gw}} \rangle &= \frac{1}{a^4} \int \frac{k^4}{2\pi^2} d \ln k \left\{ \frac{\pi}{4} (-x) [J_1(-x)^2 + Y_1(-x)^2] \right. \\ &\quad \left. - \frac{\pi}{12} (-x) [J_0(-x)^2 + Y_0(-x)^2] \right\}, \end{aligned} \quad (\text{B.29})$$

where $J_\nu(z)$ and $Y_\nu(z)$ are the Bessel functions of order ν and argument z [63, 64]. In the small argument limit, from Eqs. (B.29) we do get:

$$\langle \hat{p}_{\text{gw}} \rangle \simeq \langle \hat{\rho}_{\text{gw}} \rangle = \frac{1}{a^4} \int \frac{k^4}{2\pi^2} d \ln k \left(-\frac{1}{\pi x} \right), \quad (\text{B.30})$$

which is one of the results discussed in Section 4. Both $\langle \rho_{\text{gw}} \rangle$ and $\langle p_{\text{gw}} \rangle$ scale as a^{-6} (since $a(\tau) \sim \sqrt{-\tau}$) as it is consistent with the equation of state $\langle \hat{\rho}_{\text{gw}} \rangle \simeq \langle \hat{p}_{\text{gw}} \rangle$.

The same analysis can be performed when the energy-momentum pseudo-tensor is obtained from the quadratic corrections to the Einstein tensor. The result is

$$\begin{aligned}
\langle \hat{\rho}_{\text{gw}} \rangle &= \frac{1}{a^4} \int \frac{k^4}{2\pi^2} d\ln k \left\{ \pi [J_0(-x)J_1(-x) + Y_0(-x)Y_1(-x)] \right. \\
&\quad \left. - \frac{\pi}{4} [J_0(-x)^2 + J_1(-x)^2 + Y_0(-x)^2 + Y_1(-x)^2] \right\}, \\
\langle \hat{p}_{\text{gw}} \rangle &= \frac{1}{a^4} \int \frac{k^4}{2\pi^2} d\ln k \left\{ \pi [J_0(-x)J_1(-x) + Y_0(-x)Y_1(-x)] \right. \\
&\quad \left. - \frac{\pi}{4} x [J_0(-x)^2 + Y_0(-x)^2 + J_1(-x)^2 + Y_1(-x)^2] \right\}, \\
\langle \hat{\mathcal{P}}_{\text{gw}} \rangle - \langle \hat{p}_{\text{gw}} \rangle &= \frac{1}{a^4} \int \frac{k^4}{2\pi^2} d\ln k 4\pi [J_0(-x)J_1(-x) + Y_0(-x)Y_1(-x)]. \tag{B.31}
\end{aligned}$$

Let us now expand the previous expressions for $|x| \ll 1$. The result is:

$$\begin{aligned}
\langle \hat{\rho}_{\text{gw}} \rangle &= \frac{1}{a^4} \int \frac{k^4}{2\pi^2} d\ln k \left[-\frac{1}{\pi x} (1 - 4\gamma + 4 \ln 2 - 4 \ln(-x)) \right], \\
\langle \hat{p}_{\text{gw}} \rangle &= \frac{1}{a^4} \int \frac{k^4}{2\pi^2} d\ln k \frac{5}{3\pi x}, \\
\langle \hat{\mathcal{P}}_{\text{gw}} \rangle - \langle \hat{p}_{\text{gw}} \rangle &= \frac{1}{a^4} \int \frac{k^4}{2\pi^2} d\ln k \frac{2}{\pi x} [2\gamma - 2 \ln 2 + 2 \ln(-x)]. \tag{B.32}
\end{aligned}$$

where γ is the Euler-Mascheroni constant [63, 64]. From Eqs. (B.32) it is possible to obtain that in this parametrization of the energy-momentum pseudo-tensor, indeed, logarithmic corrections to the effective barotropic index arise, as pointed out in Section 4. From the examples reported here it is clear that also the conformal time parametrization can be employed for the self-consistent analysis of back-reaction effects. Indeed, in Section 5, explicit numerical integrations have been reported also in the τ parametrization. It is however true that, in the context of bouncing models, the σ coordinate allows to obtain the wanted results much faster both analytically and numerically.

References

- [1] L. P. Grishchuk, Zh. Éksp. Teor. Fiz. **67**, 825 (1974) [Sov. Phys. JETP **40**, 409 (1975)].
- [2] L. P. Grishchuk, Ann. (N. Y.) Acad. Sci. **302**, 439 (1977).
- [3] A. A. Starobinsky, JETP Lett. **30**, 682 (1979).
- [4] L. P. Grishchuk and M. Solokhin, Phys.Rev. D **43**, 2566 (1991).
- [5] M. Gasperini and M. Giovannini, Phys.Lett.B **282**, 36 (1992); Phys. Rev. D **47**, 1519 (1993).
- [6] V. Sahni, Phys. Rev. D **42**, 453 (1990).
- [7] V. A. Rubakov, M. V. Sazhin and A. V. Veryaskin, Phys. Lett. B **115**, 189 (1982).
- [8] R. Fabbri and M. D. Pollock, Phys. Lett. B **125**, 445 (1983).
- [9] L. F. Abbott and M. B. Wise, Nucl. Phys. **224**, 541 (1984).
- [10] G. Veneziano, Phys. Lett. B **265**, 287 (1991).
- [11] M. Gasperini and G. Veneziano, Phys. Rept. **373**, 1 (2003).
- [12] R. Brustein, M. Gasperini, M. Giovannini and G. Veneziano, Phys. Lett. B **361**, 45 (1995).
- [13] M. Galluccio, M. Litterio and F. Occhionero, Phys. Rev. Lett. **79**, 970 (1997).
- [14] M. P. Infante and N. Sanchez, Phys. Rev. D **61**, 083515 (2000).
- [15] M. Giovannini, Phys. Rev. D **58**, 083504 (1998).
- [16] Ya. B. Zeldovich and A. A. Starobinsky, Zh. Eksp. Teor. Fiz. **61**, 2161 (1971) [Sov. Phys. JETP **34**, 1159 (1972)].
- [17] L. H. Ford, Phys. Rev. D **35**, 2955 (1987).
- [18] N. D. Birrel and P. C. W. Davies, J. Phys. A **13**, 2109 (1980).
- [19] N. D. Birrel and P. C. W. Davies, *Quantum fields in curved space* (Cambridge Univversity Press, Cambridge, UK 1982).
- [20] P. J. E. Peebles and A. Vilenkin, Phys. Rev. D **59**, 063505 (1999).
- [21] B. Spokoiny, Phys. Lett. B **315**, 40 (1993).
- [22] M. Giovannini, Phys. Rev. D **60**, 123511 (1999); Class. Quant. Grav. **16**, 2905 (1999).

- [23] M. Giovannini, Phys. Rev. D **67**, 123512 (2003).
- [24] H. Tashiro, T. Chiba and M. Sasaki, Class. Quant. Grav. **21**, 1761 (2004)
- [25] D. Babusci and M. Giovannini, Phys. Rev. D **60**, 083511 (1999).
- [26] F. Y. Li, M. X. Tang and D. P. Shi, Phys. Rev. D **67**, 104008 (2003).
- [27] A. M. Cruise, Class. Quant. Grav. **17**, 2525 (2000).
- [28] P. Bernard, G. Gemme, R. Parodi and E. Picasso, Rev. Sci. Instrum. **72**, 2428 (2001).
- [29] V. Sahni, M. Sami, and T. Souradeep, Phys. Rev. D **65**, 023518 (2001).
- [30] M. Sami and V. Sahni, Phys. Rev. D **70**, 083513 (2004).
- [31] M. Sami, N. Dadhich and T. Shiromizu, Phys. Lett. B **568**, 118 (2003).
- [32] M. Yahiro, G. J. Mathews, K. Ichiki, T. Kajino and M. Orito, Phys. Rev. D **65**, 063502 (2002)
- [33] L. D. Landau and E. M. Lifshitz, *The classical theory of Fields* (Addison-Wesley and Pergamon Press, New York, 1971).
- [34] R. Isaacson, Phys. Rev. **166**, 1263 (1968).
- [35] R. Isaacson, Phys. Rev. **166**, 1272 (1968).
- [36] L. R. Abramo, R. Brandenberger, and V. Mukahanov, Phys. Rev. D **56**, 3248 (1997).
- [37] L. R. Abramo, Phys Rev. D **60**, 064004 (1999).
- [38] S. V. Babak and L. P. Grishchuk, Phys. Rev. D **61**, 024038 (2000).
- [39] L. H. Ford and L. Parker, Phys. Rev. D **16**,1601 (1977).
- [40] L. H. Ford and L. Parker, Phys. Rev. D **16**, 245 (1977).
- [41] K. A. Meissner and G. Veneziano, Mod. Phys. Lett. A **6**, 3397 (1991).
- [42] K. A. Meissner and G. Veneziano, Phys. Lett. B **267**, 33 (1991).
- [43] M. Gasperini, J. Maharana and G. Veneziano, Nucl. Phys. B **472**, 349 (1996).
- [44] J. Maharana and J. H. Schwarz, Nucl. Phys. B **390**, 3 (1993).
- [45] J. Maharana, Phys. Lett. B **296**, 65 (1992).
- [46] M. Gasperini, M. Giovannini, and G. Veneziano Phys.Lett.B **569**, 113 (2003).

- [47] M. Gasperini, M. Giovannini, and G. Veneziano Nucl.Phys. B **694**, 206 (2004).
- [48] M. Giovannini, Class. Quant. Grav. **21**, 4209 (2004).
- [49] M. Gasperini and G. Veneziano, Astropart. Phys. **1**, 317 (1993).
- [50] N. Deruelle and A. Streich, Phys. Rev. D **70**, 103504 (2004).
- [51] N. Deruelle, arXiv:gr-qc/0404126.
- [52] C. Gordon and N. Turok, Phys. Rev. D **67**, 123508 (2003).
- [53] J. c. Hwang and H. Noh, Phys. Rev. D **66**, 084009 (2002).
- [54] G. F. R. Ellis and M. S. Madsen, Class. Quant. Grav. **8**, 667 (1991).
- [55] G. F. R. Ellis and R. Maartens, Class. Quant. Grav. **21**, 223 (2004).
- [56] L. Parker and S. A. Fulling, Phys. Rev. D **7**, 2357 (1973).
- [57] A. Starobinsky, Sov. Astron. Lett. **4**, 82 (1978).
- [58] J. D. Barrow and R. A. Matzner, Phys. Rev. D **21**, 336 (1980).
- [59] C. I. Kuo and L. H. Ford, Phys. Rev. D **47**, 4510 (1993).
- [60] B. Hu and L. Parker, Phys. Lett A **63**, 217 (1977).
- [61] W. H. Press, S. A. Teutolsky, W. T. Vetterling and B. P. Flannery *Numerical recipes in Fortran 77* (second edition) (Cambridge University Press, Cambridge, UK, 1992), p.731.
- [62] V. Bozza, M. Giovannini, and G. Veneziano, JCAP **0305001** (2003); M. Giovannini, Class. Quant. Grav. **20**, 5455 (2003).
- [63] M. Abramowitz and I. A. Stegun, *Handbook of Mathematical Functions* (Dover, New York, 1972).
- [64] A. Erdelyi, W. Magnus, F. Obhehttinger, and F. Tricomi, *Higher Trascendental Functions* (Mc Graw-Hill, New York, 1953).